Evaluation of an optical technique to measure blood volume changes during hemodialysis

Master's Thesis
by
Tobias Elmhäll and **Martin Wiklund**

Lund Reports on Atomic Physics, LRAP-237
Lund, November 1998

1. Introduction

1.1 Clinical background

Patients with renal failure have today several treatment options, one of which is hemodialysis. The aim of this treatment modality is to remove excess fluid and waste products from the patient's blood, via an extracorporal flow path. The blood passes on one side of a semipermeable membrane, allowing unwanted solutes and fluid to migrate to the dialysis fluid, passing on the opposite side. The efficiency of the solute removal is influenced by the blood and dialysis fluid rates; the concentration gradients blood versus dialysis fluid and the characteristics of the membrane. The fluid removal rate is determined by the pressure gradient across the membrane and again the properties of the membrane[1]. In this work we focus on the fluid removal process. The removal of excess fluid starts a series of complicated process in the body, such as refilling from the extravascular fluid into the blood, as well as reduction in the resistance of the peripheral arteries. The biological response depends on the patient and may also vary between treatments. If the fluid removal rate is too large, the patient can end up in a state called hypovolemic shock[2]. In such a state, the blood pressure is suddenly decreased causing for example vomiting and fainting. The rapid change in blood pressure is a result of a drastic reduction of the blood volume in combination with reduced resistance of the arteries. By measuring the blood volume and simultaneously controlling the rate of fluid removal, these acute complications may be avoided and the patient can be spared a lot of suffering[3,4]. This is the most important underlying reason to the need of monitoring the blood volume in conjunction with dialysis - the objective of this work.

1.2 Measuring the blood volume

The definition of blood volume is simply the total volume of the blood of a patient. Today it is not possible to measure the blood volume directly during a dialysis process. Therefore, different techniques have been developed to measure the blood volume indirectly. The basic assumption in most methods is that the number and volume of red blood cells (RBC) remains constant during a dialysis process. It is then clear that the ratio of the cellular volume to the total blood volume, hematocrit (HCT), will change inversely with the blood volume. Thus, it is assumed that the excess fluid removed in a dialysis process is mainly taken from the plasma rather than from the cytoplasm[1].

Since we want to monitor the impact of fluid removal on the blood volume during each dialysis treatment, there is merely a need for a relative measurement versus the pre-treatment value of the blood volume. Measuring the relative change in the blood volume is a question of finding a property of the blood that changes with the blood volume changes. This can be done by a direct measurement of the HCT from a blood sample. Another parameter to be analysed corresponding to the blood volume is the hemoglobin concentration. The hemoglobin is located in the red blood cells and

therefore, the concentration of red blood cells is proportional to the hemoglobin concentration. When the blood volume decreases, the ratio of the cellular volume to the total blood volume (HCT) increases and consequently the hemoglobin concentration. Thus, there is a reciprocal relationship between the blood volume and the HCT as well as the hemoglobin concentration:

$$BV(t) = \frac{HCT(0)}{HCT(t)} \cdot BV(0) \tag{1.1}$$

$$BV(t) = \frac{Hb(0)}{Hb(t)} \cdot BV(0) \tag{1.2}$$

where

BV(t) = blood volume at time t during the treatment	(l)
BV(0) = initial blood volume	(l)
HCT(t) = hematocrit at time t	(%)
HCT(0) = initial hematocrit	(%)
Hb(t) = the hemoglobin concentration at time t	(g/l)
Hb(0) = the initial hemoglobin concentration	(g/l)

By these formulas, the relative change of the blood volume can be given by the relative change in HCT or in the hemoglobin concentration. However, such invasive methods are not preferable in a clinical perspective, since they imply a direct contact with the blood. Furthermore, for correct analysis hemolysis has to be induced and the sample can thus not be returned to the patient. To avoid this, non-invasive methods have been developed (e.g. optical, density, conductivity and ultrasonic methods[5-11]). They are based on acoustical, electrical or optical interactions with the blood i.e. indirect measurements of HCT via these properties of blood. The main advantage of such a non-invasive method is that it does not affect or change the state of the blood during the measuring procedure.

In this work we employ an optical method to indirectly monitor changes in the blood volume. The basis of the investigation was to study the light propagating straight through as well as sidewards in a cuvette with flowing blood. The possibility of building an algorithm that gives the relative blood volume from the two measured signals with good accuracy was evaluated. During a dialysis treatment, several parameters of the blood can vary such as flow rate, oxygen saturation and osmolarity. Other external parameters also matter, e.g. differences in the cuvettes used, background light and the temperature. An optimal algorithm should give the relative blood volume independent of all these parameters. We have here evaluated the formation of a ratio between the two measured signals.

Initially, suspensions of latex micro spheres and ink diluted in water with well-known optical properties were used. These measurements were performed to study the detector responses to controlled variations in the scattering and absorption properties

of a fluid, both in a qualitative and a quantitative manner. Blood measurements were then performed, while changing different parameters of interest, under circumstances similar to a dialysis treatment. Finally, comparison of the modified Hemoscan BVS to the original version (here called the BVS AK 200) as well as a commercially available BVS (Crit-Line) was performed.

Simulations of the light propagation were also performed, using a cylindrical geometry composed of a central region with a latex/ink suspension, surrounded by the cuvette (with the help of a program, Mcpipemain, obtained from Johannes Swartling, Department of Physics). The simulated results were compared to those measured.

1.3 The blood

A man that weighs 70 kg has approximately 5.6 litres of blood, i.e. 8% of the body weight consists of blood[12]. One important difference between blood and other tissues is that the cells in the blood are suspended in a liquid, called plasma. You can separate the plasma from the blood cells by centrifuging the blood. The ratio of the red blood cellular volume to the total blood volume is known as **hematocrit** (HCT), as previously mentioned. Normal hematocrit values are 39-50% for men and 34-44% for women. For dialysis patients they are less, i.e. in the order of 30-35%[1].

When the cell membrane of a red blood cell bursts or is somehow damaged, the hemoglobin will be dissolved in the plasma. This process is called **hemolysis** and occurs for instance when the blood gets in contact with pure water.

Beside plasma, the blood consists of three different types of blood cells. These four constituents of the blood will be more thoroughly discussed below.

1.3.1 The red blood cells

The main part of the blood consists of red blood cells, erythrocytes. There are approximately $5 \cdot 10^9$ per ml blood or 1000 times more than the white blood cells and 20 times more than the platelets. The red blood cells are disc shaped and biconcave at rest, but their shape is changed by external influence. The disc shaped cells have a thickness of 2-3 μm and a diameter of 7-8 μm[12]. Characteristic for human red blood cells is that they do not contain a nucleus. Its main constituent (apart from the cytoplasm) is hemoglobin.

Figure 1.1 *The shape of a red blood cell. The diameter of a real red blood cell is 7-8 μm and it has a thickness of 2-3 μm.*

1.3.1.1 Hemoglobin

The mass fraction of hemoglobin in a red blood cell is about 1/3. A normal hemoglobin concentration is 130-165 and 115-150 gram per litre blood for a male and a female, respectively. Hemoglobin is a protein consisting of four chains of peptide with place for an oxygen molecule next to an iron ion (Fe^{2+}) [13].

There are two dominating hemoglobin derivatives in our body called deoxygenated hemoglobin (reduced hemoglobin), HbR and oxyhemoglobin, HbO_2. These two derivatives are the active components of the oxygen transport in the blood. The definition for oxygen saturation is:

$$O_2sat = \frac{c[HbO_2]}{c[HbO_2] + c[HbR]} * 100 \qquad (1.3)$$

where c is the concentration of respective substance.

In the arteries, 97% of the hemoglobin is oxygenated. When the blood is transported back to the heart by the veins, the hemoglobin only binds 75% of the oxygen. The transport of carbon dioxide from the tissue to the lungs is mainly conducted by its conversion to bicarbonate by the reduced hemoglobin[12].

1.3.2 The white blood cells

The white blood cells, the leukocytes, consists of three different groups: granulocytes, lymfocytes and monocytes. There are approximately $7 \cdot 10^6$ white blood cells per ml blood, i.e. one thousandth of the number of red blood cells. In addition the number of leukocytes decreases with increasing age. All three groups of the white blood cells contain nucleus[12].

- The granulocytes can be divided into neutrophils, eosinophils and basophils, depending on what kind of granule (a small grain) there is in the plasma. These cells are about 10 μm in diameter. For instance the neutrophils defeat the bacteria when an organ has been infected.
- The lymfocytes have a diameter of 7-10 μm and play an important role in conjunction with immune reactions. They constitute 20-40% of the white blood cells.
- The monocytes are the largest of the white blood cells with a diameter of 12-15 μm. Also the monocytes can defeat bacteria.

1.3.3 The platelets

The platelets, the thrombocytes, have no nucleus and are the smallest of the cells. They have a diameter of 2-5 μm and there are approximately $150 \cdot 10^6 - 400 \cdot 10^6$ per ml in the blood. When a vessel has been injured the platelets are activated to induce blood coagulation[12].

1.3.4 The plasma

The plasma differs from other extracellular fluids due to its high concentration of protein. There are thousands of proteins in the plasma and most of them originate from the liver. Three common groups of proteins will be discussed here[12].

- Fibrinogen constitutes 5% of the plasma proteins. It is a very important factor for the clotting of the blood. When the fibrinogen has been removed from the plasma, usually by clotting, the remaining substance is called serum.
- Albumin regulates the fluid balance through the walls of the capillaries in order to maintain the osmotic pressure. The proteins in the plasma consist between 50-70% of albumin.
- Several globulines are transport proteins. Examples of common substances transported by the globulines are lipid, iron, copper and hormones. Another important group of the globulines is the immunoglobulines, the antibodies. They are a part of the immune defence and contribute with the identification of foreign substances. The immunoglobulines constitute between 10-20% of the proteins in the plasma.

1.3.5 Blood optics

Hemoglobin is the main light absorber in blood. It absorbs light in the entire visible spectral region, but dominantly in the blue and green regions rather than in for instance the red. As mentioned, there are different derivatives of hemoglobin in the blood. If the oxygen saturation is high, the principal derivative is oxyhemoglobin (HbO_2); otherwise it is in its reduced state (HbR). These derivatives have different absorption spectra shown in Figure 1.2. Certain wavelengths, so-called isobestic points, the absorbance of the hemoglobin derivatives coincide[14]. Employing probing light at these specific wavelengths enables the performance of optical measurements independent of the oxygen saturation.

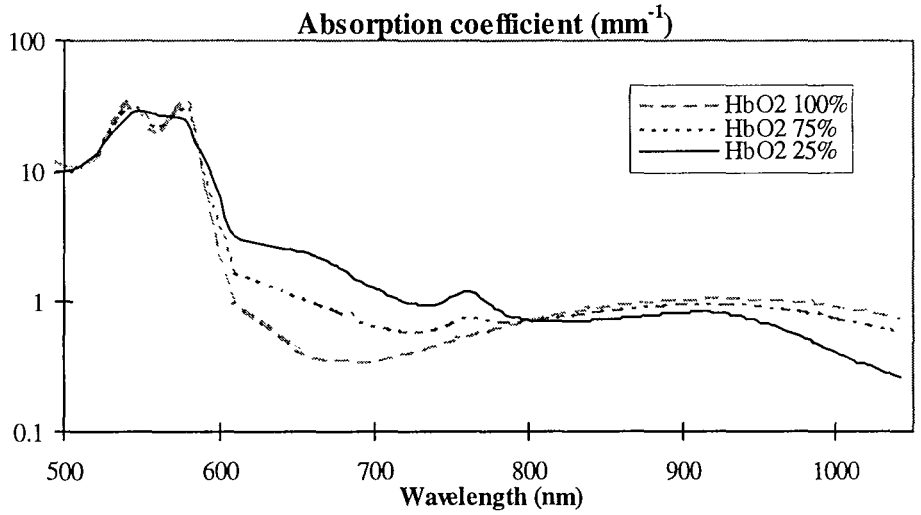

Figure 1.2 *Absorption spectra of hemoglobin with different degrees of oxygen saturation (25, 75 and 100%). At the isobestic point 800 nm, the absorption coefficient is independent of the oxygen saturation (figure obtained from A.M.K. Enejder).*

If the extinction of the light intensity, when passing through a blood sample, was only due to light absorption, there would be a simple relationship between the measured optical signal and the blood volume. However, blood is also a highly scattering medium and these effects must be taken into consideration. If a collimated light beam enters the blood, multiple scattering will occur and the collimated light will be diffusely broadened after travelling a short distance through the blood. The principal scattering objects are the red blood cells, mainly caused by the difference in refractive index of the intra- and extracellular plasma. Therefore, both the scattering and the absorption properties will change when the blood volume changes. However, there is a wide range of other parameters influencing the optical properties. For instance the scattering properties are altered if the shape or the size of the cells change[15]. As a result of this the scattering properties depend on the flow rate of blood in motion[16].

2. Theory

2.1 Light propagation in a medium

In this section we will discuss different models to describe light propagation and light interaction with a medium. This can be done by either treating light as a stream of particles, or as an electromagnetic wave. In contrast to describing light propagating in vacuum or in a gas, the particle model is most often used for medical applications. The reason for this is the dense and turbid structure of the medium being modelled here, i.e. tissue. However, from a more fundamental viewpoint, the wave properties of light should be considered, especially when describing scattering phenomena.

2.1.1 Optical properties

To quantify the light propagation, i.e. the scattering and the absorption processes, the optical parameters μ_a *(the absorption coefficient)* and μ_s *(the scattering coefficient)* are introduced[17,25]. If a photon travels a distance ds in the medium, the probability of absorption is $\mu_a ds$, and the probability of scattering is $\mu_s ds$. The dimension of μ_a and μ_s is length^{-1}, and in medical optics, the unit mm^{-1} is often used. Obviously, these optical parameters are of statistical nature, and it is therefore not adequate to use them for describing the behaviour of one single photon. The sum of the absorption and the scattering coefficient is called *the total interaction coefficient,* μ_t, i.e. $\mu_t=\mu_a+\mu_s$.

In tissue, the scattering angle is usually not averaged out, due to the asymmetric shape of the scattering objects. For example, a blood cell at rest is disc shaped and biconcave. Consequently, the angular distribution of the scattered light is also asymmetric. The asymmetry is described by the g-factor, again a parameter of statistical nature. It is defined as the average cosine of the deflection angle, θ, at scattering events. A single scattering event is described by a phase function $p(\cos\theta)$, i.e. a probability density function. The relationship between the phase function p and the g-factor is given by:

$$g = \iint_{4\pi} \cos\theta \, p(\cos\theta) \partial\Omega , \qquad (2.1)$$

where $\partial\Omega$ is an infinitesimal element of the solid angle.

There are different phase functions that are used in tissue optics, and the most common is the Henyey-Greenstein phase function. It is defined as:

$$p_{HG}(\cos\theta) = \frac{\left(1-g^2\right)}{4\pi\left(1+g^2-2g\cos\theta\right)^{3/2}}. \qquad (2.2)$$

Other phase functions have been suggested, e.g. the two-parametric Reynold-McCormick phase function:

$$p_{RM}(\cos\theta) = \frac{\alpha g}{\pi\left(\left(1+g\right)^{2\alpha}-\left(1-g\right)^{2\alpha}\right)} \cdot \frac{\left(1-g^2\right)^{2\alpha}}{\left(1+g^2-2g\cos\theta\right)^{\alpha+1}}. \qquad (2.3)$$

The definition of the g-factor is the same as in the Henyey-Greenstein phase function and the extra parameter α is a positive constant. When α=0.5, the Reynold-McCormick phase function equals the Henyey-Greenstein phase function. The value of the g-factor can in general vary between -1 *(totally back scattered light)* and 1 *(totally forward scattered light).* When g=0, the scattering is isotropic. Human tissue has a g-factor describing the zenith deflection angle, θ, in the range 0.7-0.9, it is significantly higher for blood, about 0.995. However, the latter value is not yet experimentally established. The azimuthal deflection angle, ϕ, is frequently supposed to have a uniform angular distribution for scattering in tissue, i.e. g=0. In Figure 2.1, the zenith and azimuthal deflection angles are illustated.

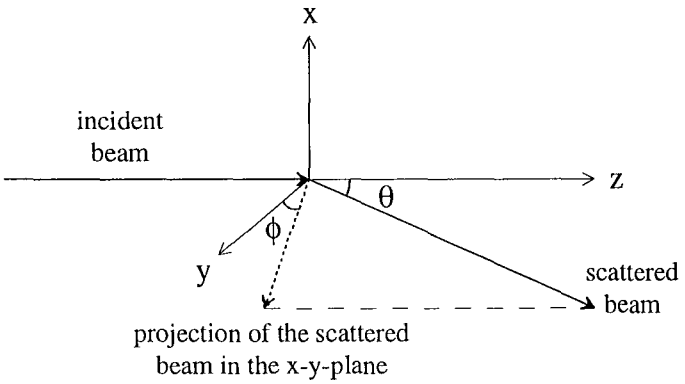

Figure 2.1 *An illustration of the angles* θ *and* ϕ*, representing the zenith and the azimuthal deflection angles, respectively, when a light beam is scattered in an arbitrary direction in space. The z-axis is chosen to be oriented in the direction of the incident beam.*

An expression for the scattering process that includes both the scattering coefficient and the asymmetry factor (the g-factor) is given by the *effective scattering coefficient* μ_s'. It is also called the *reduced scattering coefficient,* and is defined as:

$$\mu_s' = \mu_s(1-g). \qquad (2.4)$$

The reduced scattering coefficient can be regarded to represent the cumulative effect of several forward scattering events. A high value of g gives a low value of μ_s', which is the case for blood.

2.1.2 Transport theory

The transport theory treats light as a stream of particles, photons, each with a certain quantum of energy. When a photon interacts with the medium, it can either be absorbed or scattered. Only elastic scattering processes are considered, which means that the energy of the photon is conserved. The scattered photon continues to propagate at the same wavelength but in another direction. When an absorption event occurs, the photon delivers its energy to the medium and vanishes.

2.1.2.1 The radiative transport equation

A commonly used quantity to describe the number of travelling photons in a medium is the *photon distribution function* or quite simply *the number of photons,* N(**r**, **s**, t). This quantity is used when formulating the transport equation. Considering an infinitesimal volume element dV (d^3r), the photon distribution function gives the number of photons with the direction **s**, within the infinitesimal solid angle dω. The unit for N is $m^{-3}sr^{-1}$, i.e. the number of photons per volume unit and unit solid angle. Thus, in order to obtain the total amount of photons in a medium, the photon distribution function is simply integrated over all directions **s** and the total volume V. The transport equation is based on the law of energy conservation in terms of the photon distribution function. Considering a small volume dV, the balance of incoming and outgoing photons is then given by the following differential equation:

$$\begin{aligned}\frac{1}{c}\frac{\partial N(\mathbf{r},\mathbf{s},t)}{\partial t} &= -\mathbf{s}\cdot\nabla N(\mathbf{r},\mathbf{s},t) - (\mu_a(\mathbf{r})+\mu_s(\mathbf{r}))\cdot N(\mathbf{r},\mathbf{s},t) \\ &+ \mu_s(\mathbf{r})\int_{4\pi} p(\mathbf{s}',\mathbf{s})N(\mathbf{r},\mathbf{s},t)d\omega' + q(\mathbf{r},\mathbf{s},t)\end{aligned}, \qquad (2.5)$$

where c is the speed of light in the medium, and q is a source term. This equation is called the *radiative transport equation,* the fundamental equation used in the transport theory.

2.1.2.2 Beer-Lambert's law

The most simplified version of the transport equation treats the extinction of the light intensity passing through a medium as an exponential decay. In the one-dimensional case, the expression of the light intensity at the distance x in the sample is given by the Beer-Lambert's law:

$$I = I_0 e^{\mu_t x}, \tag{2.6}$$

where μ_t is the total interaction coefficient. Since μ_t is the sum of the absorption and the scattering coefficient, the Beer-Lambert's law does not consider if the extinction of the light intensity is due to scattering or absorption. Therefore, this equation is only valid if the sample thickness is small, compared to $1/\mu_t$. In a highly scattering medium, a collimated beam will be diffusely smeared out after just a few scattering events, and a more sophisticated version of the transport equation is appropriate.

2.1.3 Electromagnetic field theory

The transport equation has shown to form a useful model of the photon distribution inside tissue. However, within many applications, for instance studying the effect of cell alignment in flowing blood, this model is not sufficient. Transport theory gives no detailed information on the characteristics of each absorption and scattering event. A basic assumption in this theory is that scattering events occur at single points. This means that the effects of the complex structure of the scattering objects can not be incorporated in the model. The main scattering objects in blood are the red blood cells, and these have a dynamic geometric shape dependent on for instance the apparent viscosity and the ion concentration of the surrounding medium. If the shape of the blood cells changes, the characteristics of the scattering process also changes. Electromagnetic field theory is here a good complement to the transport equation, giving detailed information on the interaction processes of light in tissue.

2.1.3.1 Vector wave equations

The basis in the electromagnetic field theory, describing light propagation in a medium is the wave properties of light. The time-dependent complex expressions of the electric field **E** and the magnetic field **H**, which represent the propagation of a plane electromagnetic wave in a medium, are:

$$\mathbf{E}(\mathbf{r},t) = \mathbf{E}_0 e^{i(m\mathbf{k}\cdot\mathbf{r}-\omega t)} \tag{2.7}$$

$$\mathbf{H}(\mathbf{r},t) = \mathbf{H}_0 e^{i(m\mathbf{k}\cdot\mathbf{r}-\omega t)}, \tag{2.8}$$

where **k** is the propagation wave vector in vacuum, m is the complex refractive index of the medium and ω equals $2\pi f$, where f is the frequency. It is understood that the physical quantity of the electric field **E** is the real part, i.e. $\mathbf{E}_{phys}=\mathrm{Re}(\mathbf{E})$. The relationship between the electric and the magnetic fields are given by Maxwell's fundamental equations:

$$\nabla \times \mathbf{H} = \frac{1}{c}\left(\varepsilon \frac{\partial \mathbf{E}}{\partial t} + 4\pi\sigma \mathbf{E} \right) \tag{2.9}$$

$$\nabla \times \mathbf{E} = -\frac{1}{c}\frac{\partial \mathbf{H}}{\partial t}, \tag{2.10}$$

where ε is the permittivity of the medium, σ is the conductivity and c is the speed of light. If the expressions of **E** and **H** in (2.7) - (2.8) are inserted into (2.9) - (2.10), Maxwell's equations can be simplified to:

$$\nabla \times \mathbf{H} = -ikm^2 \mathbf{E} \tag{2.11}$$

$$\nabla \times \mathbf{E} = ik\mathbf{H}, \tag{2.12}$$

where the parameters k and m are defined as:

$$k = \frac{2\pi}{\lambda} = \frac{\omega}{c} \tag{2.13}$$

$$m^2 = \varepsilon + i\frac{4\pi\sigma}{\omega} \tag{2.14}$$

Obviously, k is the absolute value of the propagation wave vector **k**, also called the wave number in vacuum, and m is as previously mentioned the complex refractive index. The imaginary part of m indicates to what extent the electromagnetic wave is damped. The equations (2.11) - (2.12) can be combined and manipulated to form the *vector wave equations:*

$$\Delta \mathbf{E} + k^2 m^2 \mathbf{E} = 0 \tag{2.15}$$

$$\Delta \mathbf{H} + k^2 m^2 \mathbf{H} = 0. \tag{2.16}$$

2.1.3.2 Solution of the vector wave equations in spherical coordinates - Mie theory

The problem consists in finding the electric and magnetic fields, **E** and **H**, inside and outside the scattering object that satisfy the vector wave equations (2.15) - (2.16), with appropriate boundary conditions. If the scattering object is a homogeneous sphere, spherical coordinates can be used and the vector wave equations are separable. This problem was solved by Mie[18], resulting in solutions consisting of linear combinations of expressions containing associated Legendre polynomials, $P_n^l(\cos\theta)$, and spherical

Bessel functions, $j_n(kmr)$, or Neumann functions, $n_n(kmr)$. (The denotations are conventional standards from the literature, and l, n are indices defined as: n=0, 1, 2, ...; l=-n, -n+1, ..., n-1, n.)[18].

In Mie theory, the total electric field is divided in three parts; the incident field, $\mathbf{E}_{inc}=\mathbf{E}_{inc}(km_{inc}\mathbf{r})$, the internal field inside the sphere, $\mathbf{E}_{int}=\mathbf{E}_{i}(km_{int}\mathbf{r})$, and the scattered field, $\mathbf{E}_{sca}=\mathbf{E}_{sca}(km_{sca}\mathbf{r})$. Each field is dependent of the complex refractive index m of the medium and the wave number k. From Snell's law[19], it is known that if the refractive index is different for two mediums, a light beam deviates when passing from one to the other. This is the fundamental reason for the light scattering in Mie theory. Thus, the boundary conditions at the surface of the sphere are of vital importance for the expression of the scattered field. Conditions often used in electromagnetic field theory state that the tangential components of the electric and magnetic fields are continuous. If these conditions are combined with the general expressions of the fields that satisfy the vector wave equations, explicit expressions of the scattered field, $\mathbf{E}_{sca}$, can be derived for spheres of arbitrary sizes and with arbitrary refractive indices. When $\mathbf{E}_{sca}$ is evaluated, the far-field $\mathbf{F}$ is defined by:

$$\mathbf{E}_{sca}(km_{sca}\mathbf{r}) = \mathbf{F}(\theta,\phi)\cdot\frac{e^{ikm_{sca}r}}{r}, \tag{2.17}$$

in the limit $km_{sca}r \rightarrow \infty$. The far-field $\mathbf{F}(\theta, \phi)$ gives the scattered field at large distances from the sphere and in the direction of θ and ϕ, which are the zenith and azimuthal deflection angles, respectively. The differential normalised scattering cross section q_{sca} is then given by:

$$q_{sca}(\theta,\phi) = \left|\frac{\mathbf{F}(\theta,\phi)}{E_0}\right|^2, \tag{2.18}$$

where E_0 is the amplitude of the incident field. Thus, the differential scattering cross section expresses the amount of the incident light intensity scattered in the direction of θ, ϕ. The total normalised scattering cross section Q_{sca}, expressing the amount of the incident light intensity scattered in every possible direction, is schematically given by:

$$Q_{sca} \propto \sum q^i_{sca}, \tag{2.19}$$

where q^i_{sca} is the differential scattering cross section in the direction i. Since cross sections usually have the dimension area, the normalisation mentioned above means that the cross section σ_{sca}, is divided by the cross sectional area of the sphere, i.e.

$$Q_{sca} = \frac{\sigma_s}{\pi a^2}, \tag{2.20}$$

where a is the radius of the sphere. In this way, Q_{sca} becomes dimensionless. It can be regarded as an efficiency factor for the light scattering by the sphere and is dependent of the size and refractive index of the sphere and the wavelength of the light. It is received after summing all differential scattering cross sections q_{sca} for every combination of θ and ϕ. The g-factor, defined as the mean value of the cosine of the scattering angles, can also be calculated from the far field function $\mathbf{F}(\theta, \phi)$.

If multiple scattering is neglected, the scattering coefficient μ_s in a medium of N spheres per volume unit is given by:

$$\mu_s = N\pi a^2 Q_{sc}, \tag{2.21}$$

Due to the rather complex mathematical theory and the number of calculations needed to solve the problem with Mie theory, a computer program is frequently used. The input parameters of such a program are usually the refractive indices of the medium (m_{med}) and the sphere (m_{sphere}), the cross sectional area (πa^2) of the sphere, the wavelength (λ) of the light in vacuum and the number of spheres per volume unit (N). The output parameters are the scattering coefficient (μ_s) and the anisotropy factor (g).

Further methods for solving the vector wave equations for scattering objects of arbitrary shapes have been developed. Often, the scattering objects in tissue, e.g. blood cells, are not spherical and more sophisticated methods are appropriate, i.e. T-matrix theory[20]. This has been done for spheroidal objects, which are a better approximation of red blood cells.

2.1.4 Monte Carlo simulations

Another approach to deal with light propagation in a medium is to consider it as a number of probabilistic events. Such a method frequently used is Monte Carlo simulations. In this method, photon packages are sent out on a random walk through the medium. As in the transport equation, the light is treated as particles, i.e. photons.

2.1.4.1 Randomisation of the optical parameters

The parameters that are randomised in the Monte Carlo method are the stepsize s, the zenith deflection angle, θ, of the photon package at an interaction event as well as the azimuthal deflection angle, Φ. Each of them are associated with a probability function, p. If the random variable is denoted x, defined over the interval $a \le x \le b$, the value of x is chosen in order to fulfil:

$$\xi = \int_a^x p(x')dx', \tag{2.22}$$

where ξ is a random number between 0 and 1. If the probability function p is integrated over the whole interval (a, b), the result equals unity, i.e. ξ=1. When the probability function p is chosen and inserted into the equation (2.22), an explicit expression of x can be derived. The most frequently used probability density function is:

$$p(s) = \mu_t e^{-\mu_t s}, \quad 0 \le s < \infty, \tag{2.23}$$

for the step size where $\mu_t=\mu_a+\mu_s$,

$$p(\cos\theta) = \frac{1-g^2}{4\pi\left(1+g^2-2g\cos\theta\right)^{3/2}}, \quad 0 \le \theta \le \pi, \tag{2.24}$$

for the zenith deflection angle where g is the previously mentioned asymmetry factor and

$$p(\Phi) = \frac{1}{2\pi}, \quad 0 \le \Phi \le 2\pi, \tag{2.25}$$

for the azimuthal deflection angle.

The equation (2.24) originates from the Henyey-Greenstein phase function, as mentioned in section 2.1.1. The equation (2.23) has an exponential decay, originating from the Beer-Lambert's law, and the equation (2.25) indicates that the azimuthal deflection angle has a uniform angular distribution. If equation (2.23) - (2.25) are inserted into equation (2.22), an explicit expression for the value of each random variable can be derived:

$$s = -\frac{\ln\left(1-\xi\right)}{\mu_t}, \quad 0 \le \xi < 1, \tag{2.26}$$

for the step size,

$$\cos\theta = \frac{1}{2g}\cdot\left(1+g^2-\left(\frac{1-g^2}{1-g+2g\xi}\right)^2\right), \quad 0 \le \xi < 1, \tag{2.27}$$

for the zenith deflection angle and

$$\Phi = 2\pi\xi, \quad 0 \le \xi < 1, \tag{2.28}$$

for the azimuthal deflection angle.

2.1.4.2 The simulation procedure

When a photon package is launched, it has an initial weight, W, representing the energy of the package. Each time the package interacts with the medium, the weight W is reduced by

$$\Delta W = \frac{\mu_a}{\mu_a + \mu_s} W. \tag{2.29}$$

The procedure starts by randomising a step size, s, according to equation (2.26). The new weight is calculated as $W' = W - \Delta W$. The deflection angles are randomised using equations (2.27) - (2.28). A new step size is then randomised and the procedure is repeated until the photon exits the defined simulation area or until it is absorbed. In Figure 2.2, the simulation procedure is illustrated in a sample with the thickness d and an initial photon weight of unity.

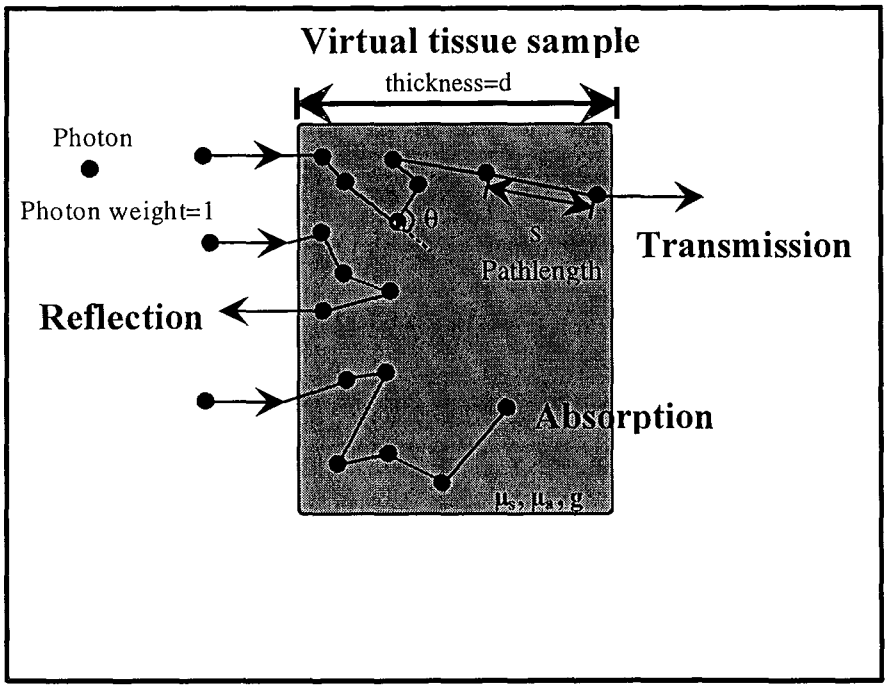

Figure 2.2 *A schematic illustration of the simulation procedure in a sample of thickness d, showing three possible simulation results; transmission, reflection and absorption of the photon package (figure obtained from A.M.K. Enejder).*

The results from a simulation can be presented in different ways. Often, the light transmission, T, is of interest, i.e. the number of photons exiting the medium at a certain surface or point, relative the total number of photons entering the medium. It is also possible to trace the history of the photons exiting the medium, e.g. how deep the reflection photons have penetrated the medium.

3. Material and methods

3.1 The Hemoscan BVS and its geometry

This work is based on an already existing non-invasive sensor, the Hemoscan BVS (Blood Volume Sensor)[21]. It probes the transmitted light through a cuvette with an inner diameter of 4 mm. The light source is an LED (Light Emitting Diode, HLP40RG, Hitachi) with a peak wavelength of 800 nm, a spectral width of 25 nm and a minimum optical power of 17 mW. A photo diode (OP913W, TRW) with a maximum response in a wide spectral range between approximately 775 and 1000 nm, is used to record the light transmission.

With the aim to develop a sensor that is less sensitive to changes in parameters other than the blood volume, the Hemoscan BVS was modified. An additional photo diode (OP913W, again) was placed perpendicular to the LED. By means of the two detectors light intensity can be measured at two different points. We hereinafter refer to them as the *side scattering, S,* and the *forward scattering, F,* light intensity. In this way, changes in the optical properties of the blood should result in different responses of the two detectors. An illustration of the modified Hemoscan sensor is shown in Figure 3.1. The diameter of the light from the LED to the cuvette and from the cuvette to the photo diode (transmission mode), respectively, is 3.5 mm. The third aperture intended for the new photo diode (side scattering mode) was chosen smaller, 1.8 mm, in order to obtain better selectivity between the two recorded signals.

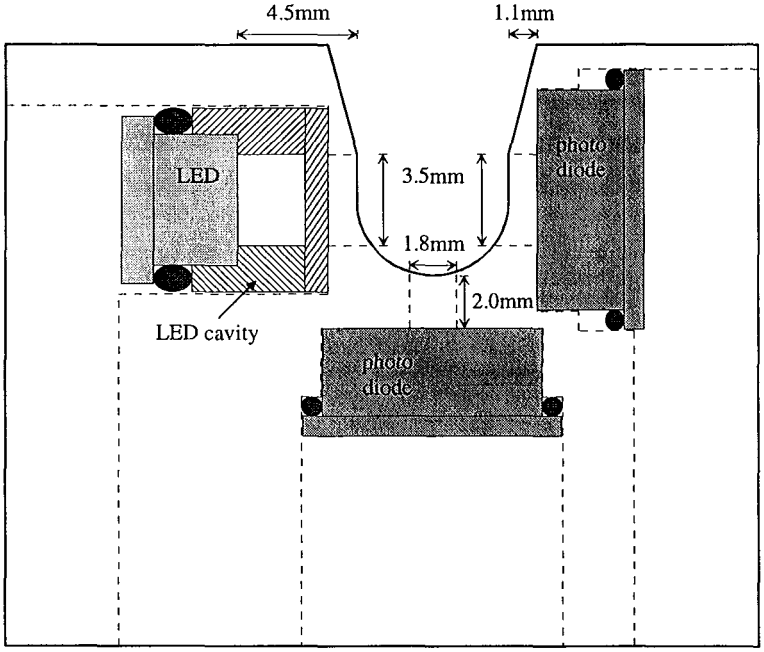

Figure 3.1 *A schematic illustration of the modified Hemoscan sensor.*

The blood was sampled by the modified Hemoscan by flowing through a specially designed cuvette, made by PVC (see Figure 3.2). The outer surface of the cuvette was shaped as a truncated cone where the diameter varied in the order of half a millimetre from one end to another. The inner surface was cylinder-shaped with a diameter of 4.00 mm. However, the precision in the manufacturing of the cuvettes did not seem to be high enough. The central axes of the two surfaces did not coincide, and accordingly the thickness of the cuvette wall varied in both angular and axial direction.

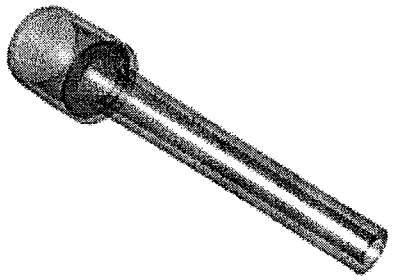

Figure 3.2 *An illustration of the specially designed cuvette.*

Since the diameter of the sensor cavity was 5.90 mm, the positioning of the cuvette was of vital importance for the stability of the sensor geometry. The cuvette was supposed to be placed in the sensor cavity with the thicker end placed in a certain holder, which in our sensor resulted in bad fitting between the cuvette and the sensor. In order to counteract this, we placed plates under the lid of the sensor. The total thickness of the plates was 0.76 mm. Furthermore, stitching paste was placed at the holder of the thick end of the cuvette. In this manner, the cuvette could be fixed to the sensor at two points, giving a stable measurement geometry assuring measurement results that can be reproduced.

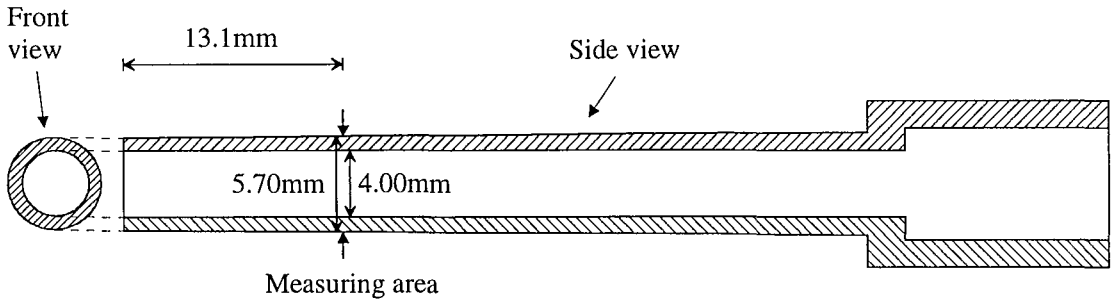

Figure 3.3 *A schematic illustration of the cuvette, side and front view. The measuring area is situated 13.1 mm from the thin end of the cuvette.*

Hardware for the signal processing and control of the Hemoscan was available[11], which, however, had to be modified in order to process the side scattering signal from the new sensor as well. This was done by using both signal systems available on the

circuit board for the Hemoscan. It has namely one control system used for the transmission signal and one protective system, now used for the side scattering signal. A master card was also available, controlling the measurement procedure and transferring the output data. It was originally constructed to alternately collect data from the Hemoscan and from another blood volume sensor, constructed in a previous diploma work. The collection of the other sensor's output was replaced by that of the side scattering signal of the modified Hemoscan (see Appendix 1.). The LED of the Hemoscan is pulsed with a frequency of 250 Hz, in order to reduce the influence of the background radiation. It was thus necessary to synchronise the recording of the side scattering signal with the LED and with the already synchronised collection of the transmission signal (see Appendix 2.).

The data from the detectors is processed by the hardware described above and then collected and displayed by a data logging program, Gambro Logging System version 1.01c. It was not possible to display the forward and side scattering signal in the same diagram without the latter being saturated, since the program handled the two signals differently. A modification (see Appendix 3.) was done to prevent this saturation.

The signals are sampled by the hardware and it generates every sixth second an average of eight sampling procedures, each consisting of eight samples. The data was collected by the data logging program and then transferred to an Excel sheet. Further, an average over 20 to 40 values was calculated for each measuring interval.

3.2 Fundamental investigations of the sensor

Some fundamental experiments were performed, in order to investigate the behaviour of the sensor. The influence of shifting and rotating the cuvette, both with and without an applicated scratch, was studied. Furthermore, the optical properties of the sensor and the sample were investigated. The suspensions used in all the experiments concerning the sensor geometry and the fundamental investigations of the sensor response, consisted of ink and microspheres of latex diluted in water. The diameter of the spheres was 2.0 μm, and the refractive index was 1.584. The main latex suspension consisted of $5.01 \cdot 10^9$ spheres per ml suspension, which was estimated from weight calibrations. The corresponding value of μ_s' can then be calculated with Mie theory. The value of μ_a was obtained with the help of a spectrophotometer (Varian), which measured the absorbency of the ink solution (Higgins). By varying the concentrations of latex and ink, the scattering and absorption coefficient could be changed independently. The pipettes used when preparing the different concentrations were carefully calibrated by weight measurements, and the margin of error was less than 1%.

3.2.1 Shift and rotation experiments

In order to examine the robustness of the results in terms of how the cuvette was positioned and due to any asymmetric shape of the cuvette, shift and rotation experiments were performed. In the shift experiments, measurements were performed

on a non-flowing latex/ink suspension with μ_a=0.83 mm^{-1} and μ_s'=0.35 mm^{-1}. The cuvette was shifted from the original position, with the plates mounted in the lid, to gradually thicker cuvette diameters at the sensor, a total displacement of 12 mm. In the rotation experiments, two different suspensions were used. First a non-scattering ink suspension (μ_a=1.1 mm^{-1}) and then a latex/ink suspension with the optical properties μ_a=0.43 mm^{-1} and μ_s'=0.67 mm^{-1}. The latter suspension was chosen to give detector values similar to those from blood measurements. In both experiments, the cuvette was rotated 360 degrees, in step of 22.5 degrees.

3.2.2 Scratch experiments

When the cuvette is not properly placed in the sensor, there is a risk of inducing damage to the PVC surface of the cuvette. Therefore, further rotation experiments were performed, but with a scratch on the cuvette. The scratch was made with a knife and had a dimension of 0.2x1.0 mm. The procedure of the rotation experiment was repeated as described previously. However, the optical properties of the latex/ink suspension were: μ_a=0.73 mm^{-1} and μ_s'=0.21 mm^{-1}.

3.2.3 The optical properties of the surface of the sensor geometry

In order to investigate the influence of the absorption properties of the inner surface of the sensor, measurements were performed with the original reflecting surface, as well as an absorbing surface. The reflecting surface was made of aluminium, i.e. the material of the sensor itself, and the absorbing surface was accomplished by covering the surface with a layer of black paint.

In the first experiment, the number of spheres per unit volume was held constant while the ink concentration was varied. The reduced scattering coefficient μ_s' was calculated to 0.385 mm^{-1}, and the absorption coefficient μ_a was varied from 0.42 mm^{-1} to 1.25 mm^{-1}, in steps of 0.104 mm^{-1}. This was performed with the aluminium surface, followed by the absorbing cavity surface. The absorption coefficient was then kept constant at μ_a=0.73 mm^{-1} whereas the reduced scattering coefficient μ_s' was varied from 0 to 0.75 mm^{-1}, in steps of 0.075 mm^{-1}. As in the absorption experiments, both a reflecting and an absorbing sensor geometry were investigated.

Finally, the absorbing and the reflecting properties of the cavity were tested on samples consisting of flowing (flow rate about 300 ml/min) blood with different hemoglobin concentrations. Two series were performed at different occasions on different blood batches, the hemoglobin values, and thus the optical properties, do not match properly. In the aluminium series, the total amount of hemoglobin was varied between 70-135 g/l, and in the absorbing-cavity series, the corresponding interval was 55-95 g/l. The last data in each series originate from measurements on the whole blood and the others after diluting the blood with NaCl solutions (0.9%).

3.2.4 The optical properties of the sample

In order to relate the response of the sensor to samples with well-known optical properties a more thorough investigation of variations in both the absorption and the scattering coefficient was conducted. The reduced scattering coefficient of the latex/ink suspension was varied from 0.20 to 0.50 mm^{-1}, in steps of 0.033 mm^{-1}, and the absorption coefficient from 0.50 to 1.00 mm^{-1}, in steps of 0.056 mm^{-1}. Thus, ten different scattering series, each with a specific and constant absorption coefficient, were achieved. Totally, measurements on hundred suspensions with different combinations of μ_a and μ_s' were performed. The same cuvette was used in all measurements.

The results of the measurements were compared with those obtained from Monte Carlo simulations. They were performed, using a specially designed program (the program, Mcpipemain, was obtained from Johannes Swartling, Department of Physics) with a geometric model of the sensor and the cuvette (see Figure 3.4)

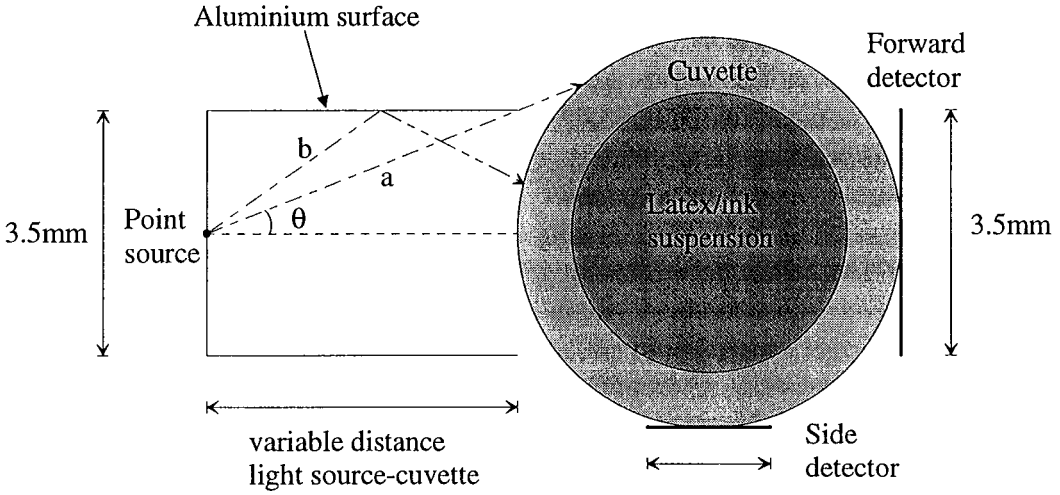

Figure 3.4 *An illustration of the simulation geometry. Photon (a) reaches the cuvette without any reflection, while photon (b) is reflected in the aluminium surface of the light source cavity. The angle* θ *indicates the maximum angle for no reflection.*

The cuvette was modelled as a two-layer cylinder. The optical properties of the layers, i.e. latex/ink suspensions and the PVC cuvette walls, were defined according to data shown in Table 3.1.

Table 3.1 *Optical properties used for the Monte Carlo simulations*

	d (mm)	n	μ_a (mm^{-1})	μ_s' (mm^{-1})	g
Layer above (air)	-	1.00	-	-	-
Layer 1 (PVC)	0.8	1.56	0	0	1
Layer 2 (latex/ink)	2.0	1.33	0.50-1.00	2.90-7.25	0.93103

Source cavity diameter:	3.5 mm
Detector diameter (side scattering):	1.8 mm
Detector diameter (forward scattering):	3.5 mm
Distance source - cuvette:	3.4 mm
Divergence angle of the source:	$2x60^{\circ} = 120^{\circ}$
Inner diameter of the cuvette:	4.0 mm
Outer diameter of the cuvette:	5.6 mm

The light source was assumed to be a point source and the angular distribution of the photons was gaussian with a width of 120 degrees. The maximum angle θ allowing the photons to reach the cuvette without any reflection in the aluminium surface is illustrated in Figure 3.4, by the light beam (a). If the angle is greater than θ, the photon will be reflected of the aluminium surface of the light source cavity (illustrated by light beam (b) in Figure 3.4. When a photon reaches the aluminium surface, the reflectance R gives the probability of reflection, and the angular distribution after the reflection was assumed to be isotropic. The photons transmitting through the PVC layer of the cuvette out in the surrounding layer (air) were assumed to be absorbed, in accordance with the absorbing cavity geometry. Thus it was not possible to simulate the aluminium cavity geometry. Simulations were performed with the same optical parameters of the latex/ink suspensions as used in the measurements. In all, hundred different simulations were performed using 100 000 photons in each run.

3.3 Simulated dialysis experiments

The aim was to simulate a blood flow from a patient under the same circumstances as when the blood volume is measured during a dialysis process. Fresh bovine blood was delivered from scan in a 10-litre can. 10 ml of Heparin, was added in order to prevent coagulation. At every delivery the hematocrit of the blood was evaluated. A small amount of the blood was centrifuged in a capillary tube and then the length of volume occupied by the red blood cells was measured and divided by the total length of the volume filled with blood. The blood was never older than 2 days and stored in a refrigerator when not being used.

3.3.1 Experimental set-up

During the experiments on blood, two kinds of fundamental set-ups were used and they in turn were modified differently to suit every specific experiment. The first set-up, shown in Figure 3.5, was used for thorough investigations of the modified Hemoscan sensor. A beaker filled with 400 ml blood was placed in a warm water bath and gently stirred with a magnetic stirrer. The temperature on the blood (37 °C) was measured by a temperature meter, Testo 110 Nordtec Instrument, and then registered manually. A roller pump pulled the blood from the beaker through the modified Hemoscan sensor and then pumped it back to the beaker again. The blood was flowing through tubes with an integrated cuvette, which was placed in the modified Hemoscan sensor. An OSM3 Hemoximeter (Radiometer, Copenhagen) was used to analyse blood samples in terms of tHb (g/l), HbO_2 (%), HbCO (%), MetHb (%) and O_2ct (%)

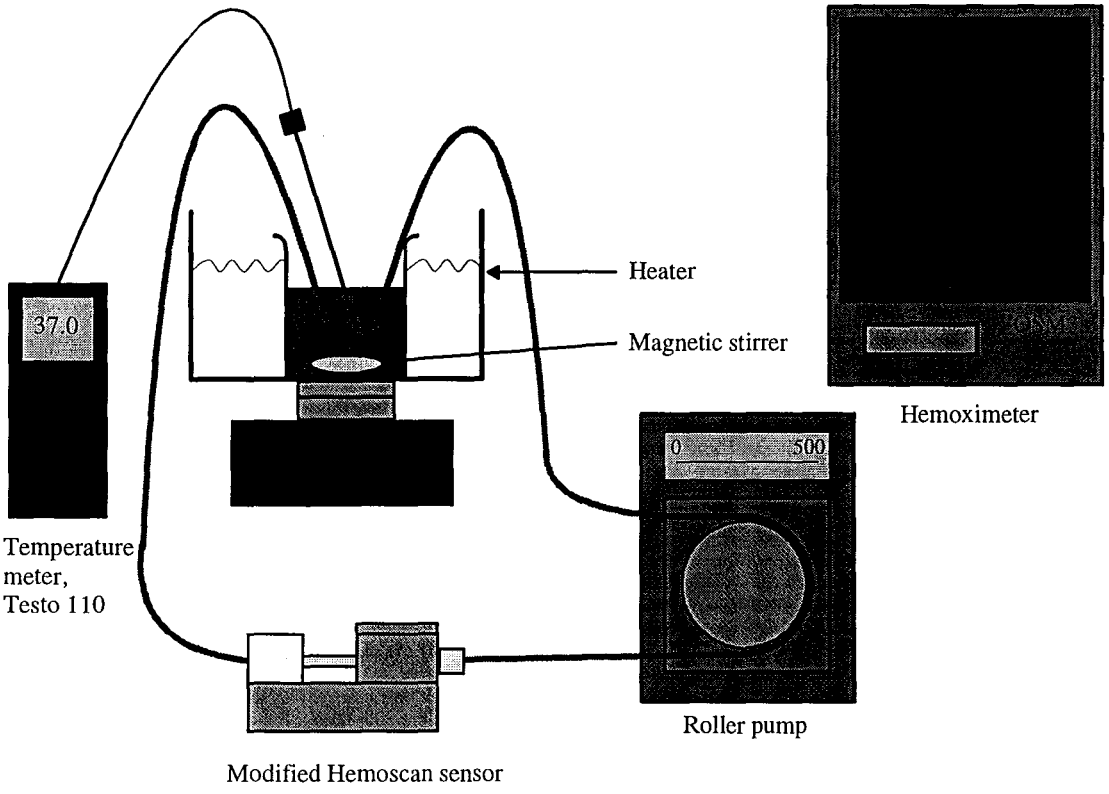

Figure 3.5 *The fundamental set-up used during the investigations of the modified Hemoscan sensor.*

The second set-up, shown in Figure 3.6, was used in order to compare the performance of the modified Hemoscan with that of a blood volume sensor (BVS) from Gambro, originating from the Hemoscan, and a commercial, the Crit-Line. In these experiments the modified Hemoscan sensor was connected in series with these. The Gambro BVS was mounted on a dialysis machine, AK 200, immediately after the roller pump, followed by the modified Hemoscan sensor and finally the Crit-Line. Three different kinds of cuvettes were used. The cuvette intended for the Crit-Line sensor has a circular disc shaped geometry in contrast to the conical cylinders used as

cuvettes for the other two sensors. Furthermore, the length of the cuvette for the BVS AK 200 is half that of the cuvette used for the modified Hemoscan sensor.

The data acquisition of the BVS AK 200 was performed by the dialysis machine and then fed into a computer. The logging program, Gambro Logging System version 2.08, also collected data synchronously from the Crit-Line and the modified Hemoscan sensor.

The ends of the blood tubes were placed in a beaker filled with 500 ml of blood. The beaker was placed in a water bath in order to maintain a stable temperature at 37 °C. The temperature was monitored by the same temperature meter used in the previous set-up.

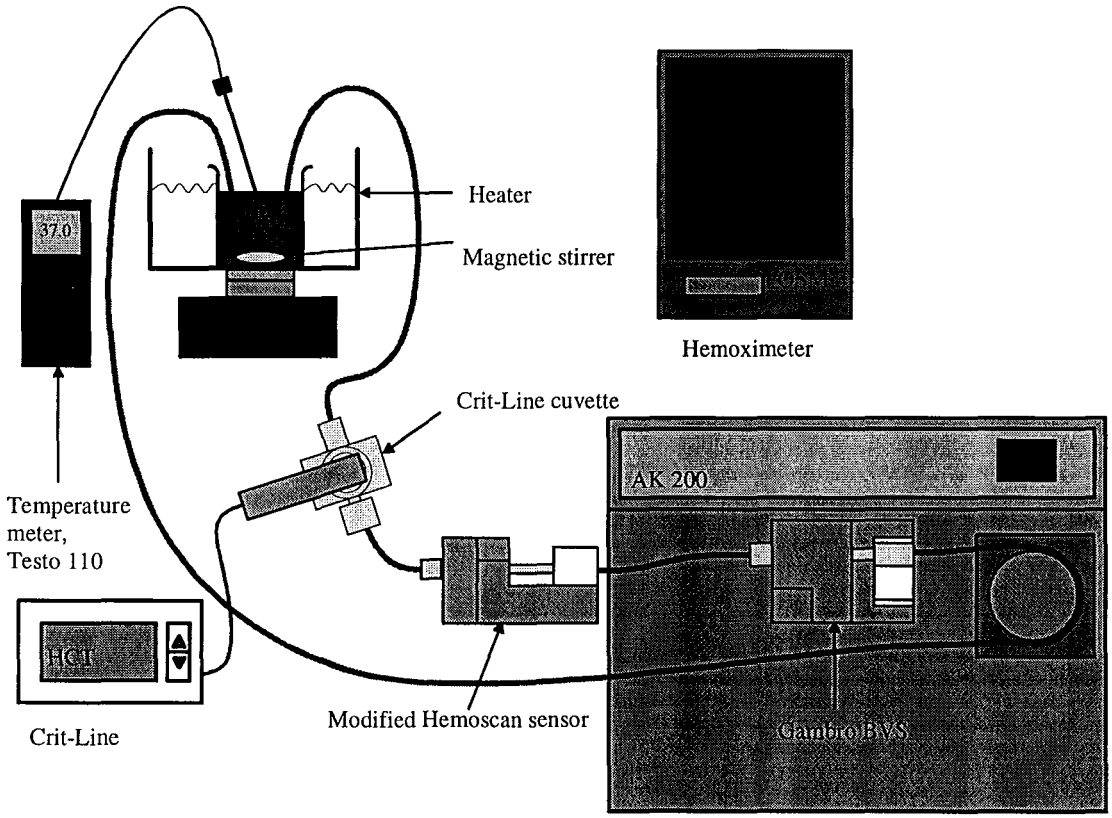

Figure 3.6 *A schematic outline of the set-up used to measure the signals synchronously from the three different sensors.*

3.3.2 Optimisation of the experimental set-up

A few experiments were performed to investigate whether it was possible to improve the experimental arrangement. Since the Hemoscan sensor is vertically mounted, i.e. the blood is flowing downwards instead of sidewards, on a dialysis machine (Integra) from Hospal, this difference in the arrangement was examined. The degree and influence of hemolysis of blood was also investigated.

When comparing horizontal versus vertical geometry of the modified Hemoscan, the measurements lasted for half an hour each. The measurements were performed at blood flow rates of 200 ml/min and 300 ml/min. The mean value of the amount of hemoglobin was 125 g/l and the hematocrit value was 38.5%. The mean value of the oxygen saturation was 29 and 27% for the vertical and horizontal geometry, respectively.

Furthermore, we evaluated whether the use of a mini-oxygenator as well as the size of connectors between tubes, increased the degree of hemolysis in the experimental set-up. The degree of hemolysis was in all these experiments analysed by centrifuging the blood samples and thereafter measuring the absorbance, at the wavelength 418 nm, of the plasma with a spectrophotometer, called Cary 50 Scan (Varian).

When evaluating the influence of a mini-oxygenator, a drip chamber with a filter and the oxygenator itself was added to the first set-up. They were placed after the roller pump with the drip chamber before the mini-oxygenator. The purpose of the mini-oxygenator, with the help of a flowing gas mixture (95% O_2 and 5% CO_2), was to raise the oxygenation of the bovine blood. To prevent coagulation in the oxygenator a drip chamber with filter was needed. The mean value of the total hemoglobin was 84 g/l and the hematocrit was approximately about 25%. A blood flow rate of 350 ml/min was used during the measurements and the oxygen saturation maintained between 96 and 97%.

The experiment contained three measurement series. The first one lasted for one hour with one blood sample taken every tenth minute. Another two similar measurements were then performed, each during half an hour. Blood samples were here taken every sixth minute. Between the measurements the set-up was flushed with a 0.9% NaCl solution.

When investigating the influence of the size of the tube connectors three types of arrangement were used. The first experiments were performed with narrow connectors (inner diameter = 1.2 mm) between the tubes. The narrow connectors were then exchanged by connectors with the same inner diameter (4.5 mm) as the tubes.

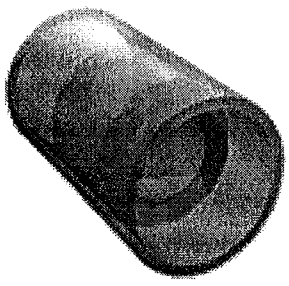

Figure 3.7 *The shape of a large connector. The smallest inner diameter is 4.5 mm.*

Finally, using the wider connectors, a mini-oxygenator was added to the set-up, but no drip chamber. Summarising, the measurements performed were:

- A set-up with narrow connectors and blood flow rates of 414 ml/min (O_2sat=25%) and 299 ml/min (O_2sat=22%). The mean value of the total hemoglobin was 111 g/l and the hematocrit was 35.3%.

- A set-up with large connectors and blood flow rates of 473 ml/min (O_2sat=18%) and 350 ml/min (O_2sat=22%). The mean value of the total hemoglobin was 112 g/l and the hematocrit was 35.3%.

- A set-up with large connectors and a mini-oxygenator. Measurements were performed at a blood flow rate of 469 ml/min (O_2sat=97%). The mean value of the total hemoglobin was 114 g/l and the hematocrit was 35.3%.

Each experiment lasted for one hour and afterwards a blood sample was taken and centrifuged. The plasma for each of the samples was analysed in the spectrophotometer and thus the degree of hemolysis.

3.3.3 Experimental procedure

Every experiment began by flushing the material and the tubes with a 0.9% NaCl solution. Then the blood was flowing through the tubes until the oxygenation of the blood was stabilised. This was determined by analysing a blood sample using the Hemoximeter, giving a value of HbO_2 (the relative concentration of oxyhemoglobin) In addition, the real measurements did not start before the blood was heated to about $37\,^{\circ}C$. During the measurements, blood samples were continuously taken from the beaker (when the blood samples were taken from the measuring site it affected the optical signals too much due to bubbles) and then analysed in the Hemoximeter. The results of these analyses were continuously noted along with the blood temperature as well as with the recording.

3.3.3.1 Hemoglobin experiments

In order to investigate the modified Hemoscan sensor, the side and forward scattering light were measured as a function of the hemoglobin concentration of bovine blood. These experiments were divided into two parts, one of which had the intention to imitate measurements on human blood with high degree of oxygenation.

The first set-up (see Figure 3.5) was used in the initial experiment and at a blood flow rate of 300 ml/min and an oxygen saturation of 35%. The whole blood had a total hemoglobin concentration of 121 g/l (HCT=37.5%) and it was diluted to different concentrations of hemoglobin (65, 74, 83, 95, 101 and 111 g/l) using a 0.9% NaCl solution.

In the other experiment, whole blood with the total hemoglobin concentration of 146 g/l (HCT=44.5%) was available, which is similar to normal human blood. The whole blood was diluted in the same way as for the first experiment (83, 94, 104, 124 and 135 g/l). In order to imitate human blood, it was oxygenated to 96.4%. This was done by placing a mini-oxygenator after a drip chamber and the roller pump.

The influence of the hemoglobin concentration was also investigated using the second set-up (see Figure 3.6), i.e. the three different sensors connected in series was used in these experiments. The transmitted intensity was measured by the BVS AK 200 and both the side and forward scattering signals were measured by the modified Hemoscan sensor, with the intention to investigate their behaviour in comparison to that of the Crit-Line.

The hematocrit value of the whole blood was 40.9%, which corresponded to a total hemoglobin value of 141 g/l. The blood was diluted with plasma to different concentrations of hemoglobin (91.5, 104, 118 and 131.5). The plasma was produced by centrifuging the blood in twelve 50 ml test tubes for 35 minutes with a rotation speed of 4000 rpm at a temperature of 4 °C. The optical measurements were performed at a blood flow rate of 308 ml/min and with an oxygenation of the blood between 27 and 36% for all the concentrations, except for the whole blood, which had an oxygen saturation of 18%.

3.3.3.2 Oxygen saturation experiments

In order to study the change of the signals during the oxygenation of the blood, a mini-oxygenator was mounted after the roller pump (see Figure 3.5). However no oxygen was flowing in the mini-oxygenator in order to obtain a slow oxygenation process. Between the roller pump and the oxygenator a drip chamber with a filter was placed.

A blood sample was taken every second minute and the blood flowed in the tubes at a flow rate of 300 ml/min. The total hemoglobin value and the hematocrit was 127 g/l and 39%, respectively. The measurements lasted for 26 minutes.

3.3.3.3 Osmolarity experiments

When investigating the modified Hemoscan sensor, the first set-up (see Figure 3.5) was used to measure the dependence between the osmolarity of the blood and the change in side and forward scattering light.

The whole blood had a hematocrit value of 39%, but was diluted to approximately 30%. The hematocrit value changes when the osmolarity changes, since the volume of the cells varies due to the equalisation of the osmotic pressure changes. The total hemoglobin value on the other hand, remains constant. Five beakers of whole blood were diluted with five different concentrations (0.7-1.1%) of NaCl solutions resulting in NaCl concentrations in the blood of 0.85, 0.88, 0.9, 0.92 and 0.95%. The total

hemoglobin value was measured to 99 g/l in all the diluted blood samples. The blood flow rate used was 305 ml/min and the blood was oxygenated to approximately 30%.

The arrangement with all the three sensors (see Figure 3.6) was then used, in order to compare their behaviour when the concentration of NaCl was varied.

The whole blood had a hematocrit value of 40.9% and was diluted to approximately 30%, which corresponded to a total hemoglobin concentration of 103 g/l. Six different concentrations of NaCl solution were prepared, 0.53, 0.65, 0.78, 0.90, 1.02 and 1.15%, in order to achieve the following NaCl concentration of the blood: 0.8, 0.83, 0.87, 0.9, 0.93 and finally 0.97%. The measurements were performed at the blood flow rate 308 ml/min and lasted for approximately 20 minutes for each concentration. The oxygen saturation of the blood concentrations was between 22 and 24%.

3.3.3.4 Flow rate experiments

The change of the side and forward scattering signals from the modified Hemoscan sensor, were studied as a function of the flow rate at three different values of total hemoglobin. The first set-up (Figure 3.5) was used with the same blood tubes for all the measurements.

Prior to the measurements, a calibration of the roller pump was done by measuring the time with a stopwatch for the blood to fill a 50 ml test tube. All the experiments began by measuring at the lowest blood flow rate (77 ml/min), increasing the highest flow rate to 469 ml/min. To confirm the reproducibility of the dependence between the signals and the flow rate, the measurements were also performed with decreasing flow rates, starting at the highest value. The experiments with the three different blood concentrations lasted each for one hour under the following conditions:

1. In the first experiment the total hemoglobin value was 84 g/l corresponding to a hematocrit of 25%, and the oxygenation of the blood was approximately 35%.
2. In the second measurement series the total hemoglobin value was 114 g/l with a hematocrit of 35% and an oxygenation of the blood of 31%.
3. In the last experiment the total hemoglobin value was 143 g/l, corresponding to a hematocrit of 44.5% and the oxygenation of the blood was approximately 18%.

Using the second set-up (see Figure 3.6), the influence of the flow rate on the signals of the other sensors was investigated as well. The roller pump mounted on the AK 200 was in these experiments utilised in order to vary the flow rate within a range of 25 to 484 ml/min.

Two similar experiments were performed for two blood samples with different hematocrit values, 37.5 and 31.3%. Blood samples with lower HCT were obtained by diluting with plasma from centrifuged whole blood. The centrifugation lasted for 35 minutes and was again done with a rotation speed of 4000 rpm at the temperature 4°C. The centrifuge had the possibility to take 12 tubes, each with the volume 50 ml, at the same time.

In the first series of experiments the whole blood with the total hemoglobin concentration of 117 g/l, corresponding to a hematocrit of 37.5%, was used. It had an oxygen saturation of approximately 32% and the measurements lasted for 53 minutes. Thereafter the whole blood was diluted to a total hemoglobin concentration of 100 g/l with a hematocrit value of 31.3%. During this experiment the oxygen saturation was approximately 43% and the measurement time was 53 minutes. The last hemoglobin concentration used was 81 g/l, which corresponded to a hematocrit value of 25%. This measurement series lasted for 50 minutes and the oxygen saturation was approximately 42%.

The second series of measurements were performed with another batch of whole blood. It had a total hemoglobin concentration of 101 g/l and a hematocrit value of 31.3%. The measurement time was 65 minutes and the oxygen saturation approximately 30%. The next concentration, 91 g/l, corresponded to a hematocrit value of 28.1%. In this case the blood had an oxygen saturation of approximately 35% and the measurements lasted for 52 minutes. The final experiment was performed on a hemoglobin concentration of 81 g/l, corresponding to a hematocrit value of 25%. The blood had an oxygen saturation between 35 and 45%. The measuring time was 58 minutes.

In order to investigate the slope of the flow rate curves versus the hemoglobin concentration, a linear fit of the data in the curves was performed. The data was registered by the sensors and then an average was calculated for each flow rate. The linear function was fitted to these averages in the flow rate range 177-308 ml/min and then repeated for six blood samples with different concentrations.

4. Results

4.1 Fundamental investigations of the sensor

In this section, the results from all fundamental investigations of the sensor will be presented. The measurements were usually performed on water suspensions of latex and ink diluted with well-defined optical properties (if so, clearly specified in the figure legends), but blood is also used in some cases.

4.1.1 Shift and rotation experiments

When the cuvette is shifted along its main axis, the thickness of the cuvette wall is changed. In Figure 4.1, the thickness of the wall increases with increasing shift. We can see that the detected signals decrease when the thickness of the wall increases, especially the forward scattering signal (approximately 25%/cm). The results were also analysed by forming a ratio between the side and forward scattering signals. Wall thickness dependent changes in the ratio are small for lateral shift in the interval 0-5 mm, but significant at larger shifts. For instance, the ratio increases by 15% at a shift of 1 cm.

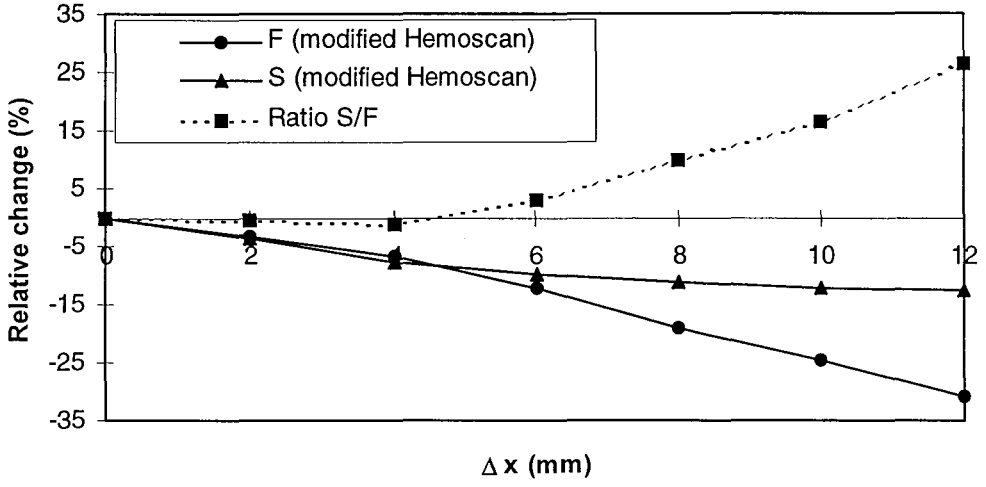

Figure 4.1 *The change in the side (S) and forward (F) scattering signals, as well as in the ratio S/F, are displayed relative to the values obtained when the cuvette is placed in its initial position (x=0). The data are shown as a function of the lateral shift (Δx) of the cuvette and the measurements were performed with the optical properties:* μ_a*=0.83 mm*$^{-1}$ μ_s'*=0.35 mm*$^{-1}$*. All standard deviations are within the range of the symbols.*

In Figure 4.2 and Figure 4.3, results from the measurements on a non-scattering ink solution is shown versus the rotation angle of the cuvette, and Figure 4.4 displays the

results from measurements on a latex/ink suspension with optical properties closer to those of blood. Thus, the non-scattering ink solution merely demonstrates the qualitative behaviour, while the measurements on the suspension were meant to indicate a quantitative behaviour comparable to measurements on blood.

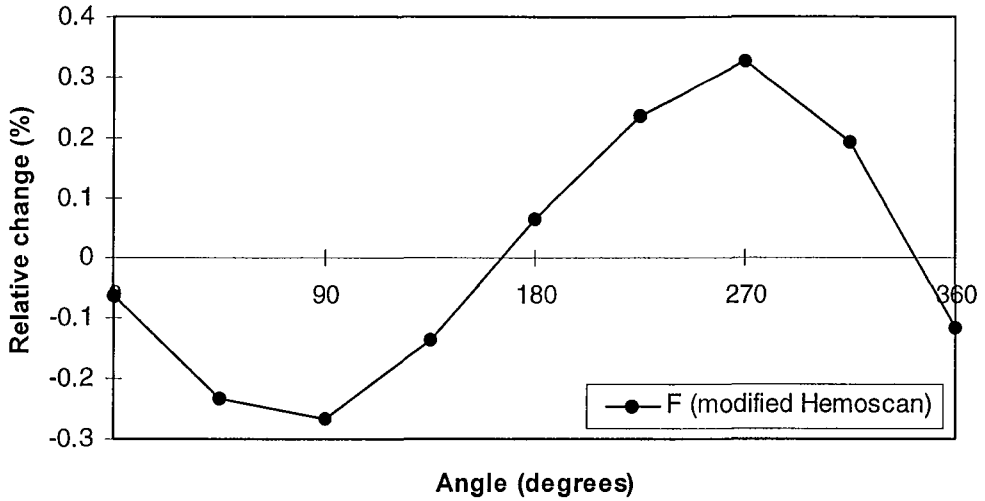

Figure 4.2 *The relative change in the forward (F) scattering intensity in comparison to the mean value, is shown as a function of the rotation angle of the cuvette (μ_a=1.1 mm^{-1}, μ_s'=0). The standard deviations are within the range of the symbols.*

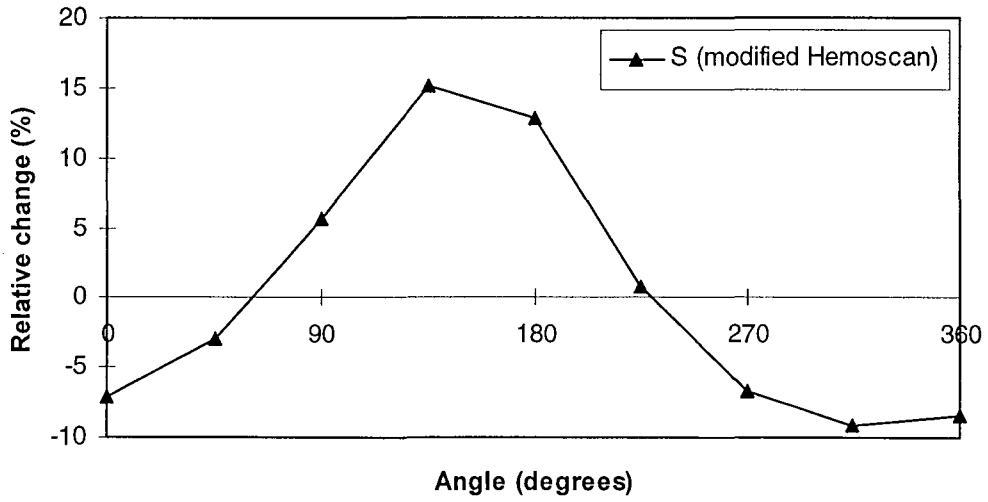

Figure 4.3 *The relative change in the side (S) scattering intensity in comparison to the mean value, is displayed as a function of the rotation angle of the cuvette (μ_a=1.1 mm^{-1}, μ_s'=0). All standard deviations are within the range of the symbols.*

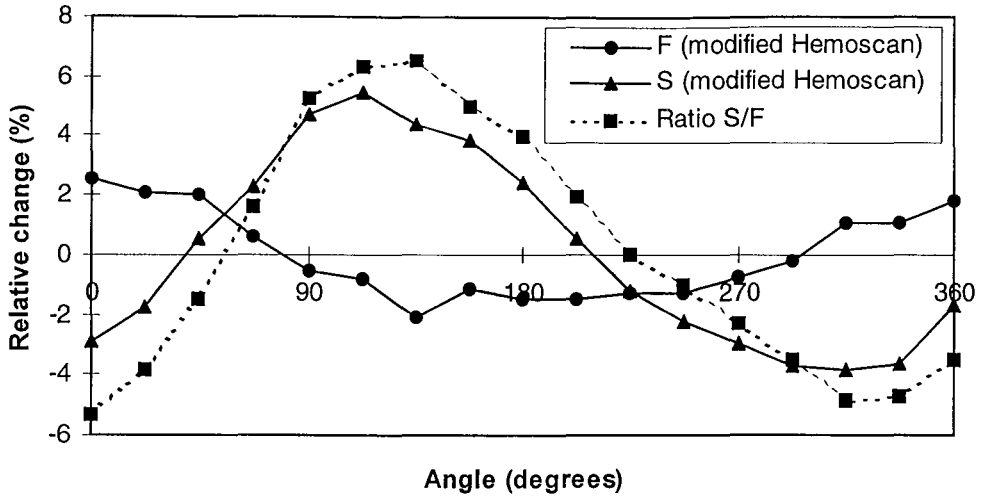

Figure 4.4 *The relative change in the side (S) and forward (F) scattering intensities, as well as in the ratio S/F, relative to the mean value, are shown as a function of the rotation angle. Here the measurements were performed on a latex/ink suspension, with the absorption coefficient 0.43 mm^{-1}, and the effective scattering coefficient 0.67 mm^{-1}. The standard deviations are in the range of the symbols.*

The recorded signals all have a sinusoidal shape, and the phase shift between the side scattering and the forward scattering signals is approximately $\pi/2$, i.e. the same as the angle between the detectors. The forward scattering signal varies about $\pm 2\%$ round its mean value, and the side scattering signal varies approximately $\pm 5\%$. The ratio of the side to the forward scattering light varies slightly more, in the order of $\pm 6\%$.

4.1.2 Scratch experiments

When a cuvette with a scratch was rotated in the sensor, the sinusoidal shape of the curves shown in Figure 4.2 - Figure 4.4 is lost. This is clearly seen in Figure 4.5 and Figure 4.6. The scratch on the surface of the cuvette is in front of the forward scattering detector at 67.5 degrees, the side scattering detector at 157.5 degrees and the LED at 247.5 degrees. The reference signal was recorded with the same cuvette in the sensor, but without the scratch.

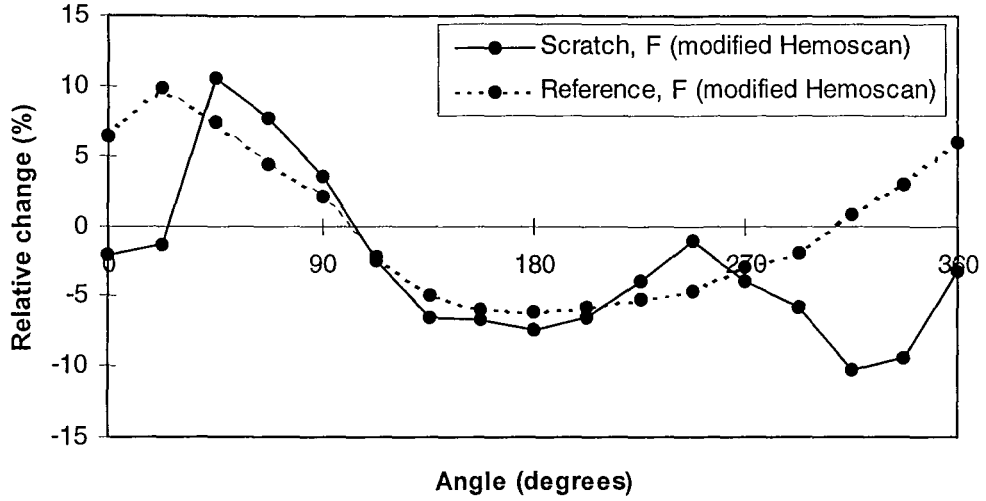

Figure 4.5 *The relative change in the forward (F) scattering intensities in comparison to the mean value of the reference signal, are shown as a function of the rotation angle. The reference signal is measured under the same conditions, but before the application of the scratch (μ_a=0.73 mm^{-1}, μ_s'=0.21 mm^{-1}). The standard deviations are within the range of the symbols.*

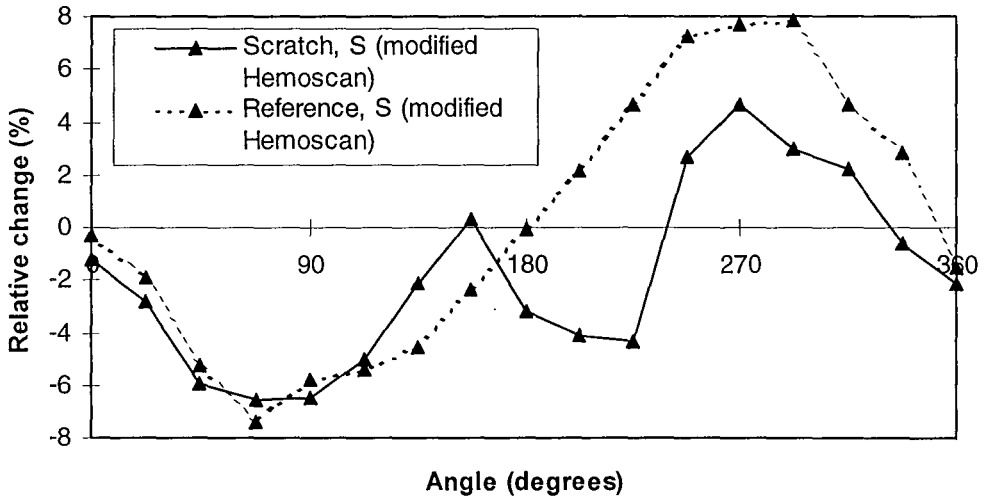

Figure 4.6 *The relative change of the side (S) scattering intensities in comparison to the mean value of the reference signal, are shown as a function of the rotation angle. The reference signal is measured under the same conditions, but before the application of the scratch (μ_a=0.73 mm^{-1}, μ_s'=0.21 mm^{-1}). All standard deviations are within the range of the symbols.*

4.1.3 The optical properties of the cavity surface

The following diagrams present the results from the sensor cavity experiments, i.e. when comparing the results obtained with a reflecting and an absorbing inner sensor surface. In Figure 4.7 - Figure 4.10, the detector signals are plotted versus the optical

properties of different latex/ink suspensions, and in Figure 4.11 and Figure 4.12, the signals are plotted versus the hemoglobin concentration of blood.

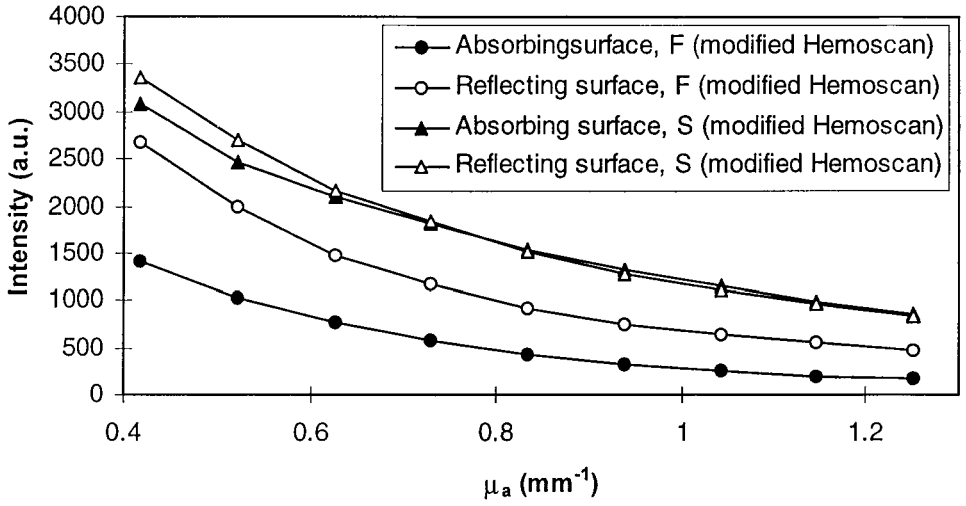

Figure 4.7 *The side (S) and forward (F) scattering intensities are plotted versus the absorption coefficient* μ_a *of the latex/ink suspension* (μ_s'*=0.385 mm*$^{-1}$*), measured with an absorbing as well as a reflecting cavity surface. All standard deviations are within the range of the symbols.*

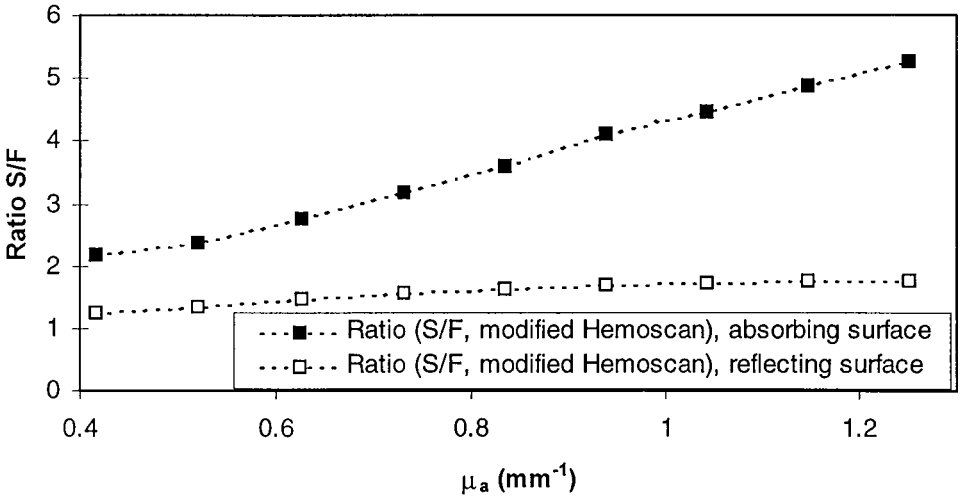

Figure 4.8 *The ratio between the side (S) and forward (F) scattering intensities, shown in Figure 4.7, is shown versus the absorption coefficient* μ_a (μ_s'*=0.385 mm*$^{-1}$*), measured with an absorbing as well as a reflecting surface. The standard deviations are within the range of the symbols.*

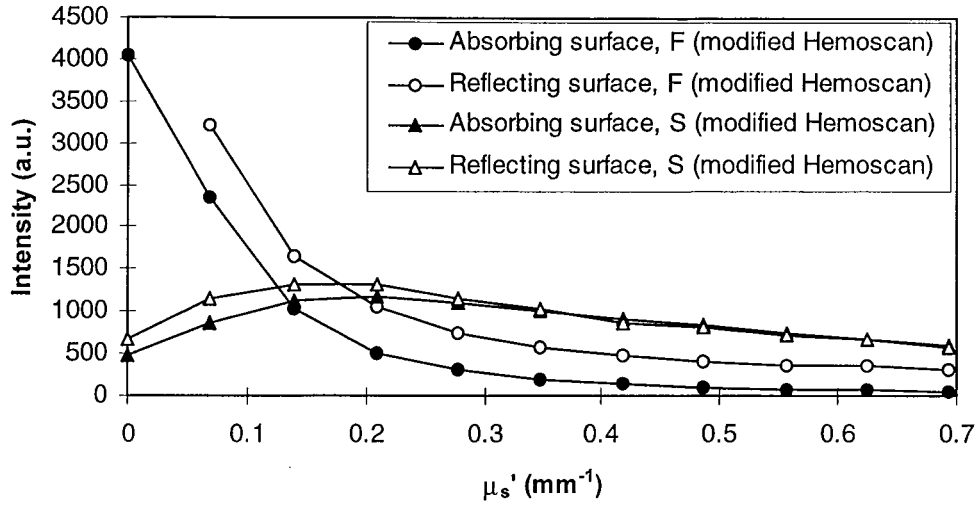

Figure 4.9 *The side (S) and forward (F) scattering intensities are displayed versus the effective scattering coefficient μ_s' of the latex/ink suspension (μ_a=0.73 mm^{-1}), measured with an absorbing as well as a reflecting cavity. All standard deviations are within the range of the symbols.*

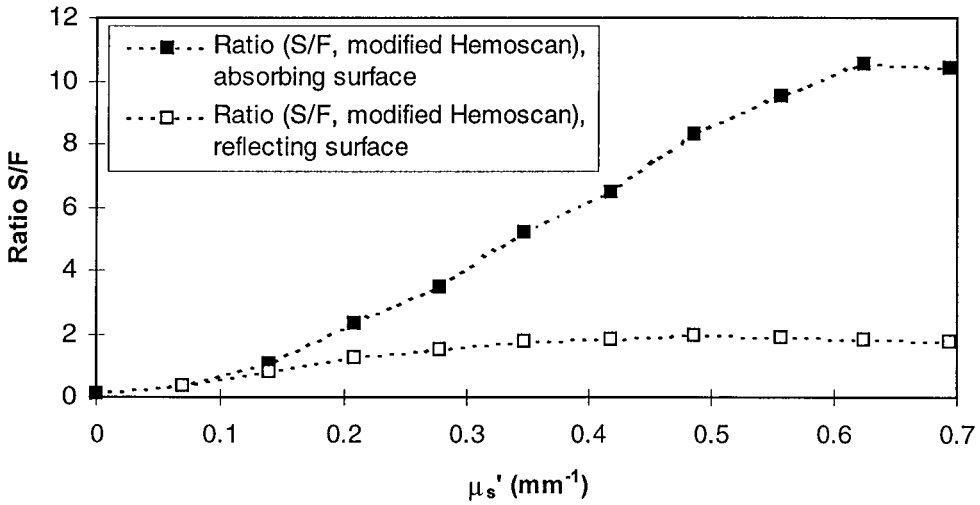

Figure 4.10 *The ratio between the side (S) and forward (F) scattering signals, shown in Figure 4.9, is plotted versus the effective scattering coefficient μ_s' (μ_a=0.73 mm^{-1}). A comparison between an absorbing and a reflecting surface of the sensor cavity. The standard deviations are within the range of the symbols.*

Figure 4.8, Figure 4.10 and Figure 4.12, display a stronger dependence of the optical properties as well as of the hemoglobin concentration in the ratio when the cavity surface is absorbing in compared to that obtained with reflecting cavity surface. This is particularly clear for the blood measurements (Figure 4.12). In the latter experiment, the ratio is doubled when the hemoglobin concentration is doubled for an absorbing cavity surface. For a reflecting cavity surface, the ratio increases with 30% at the corresponding tHb increase.

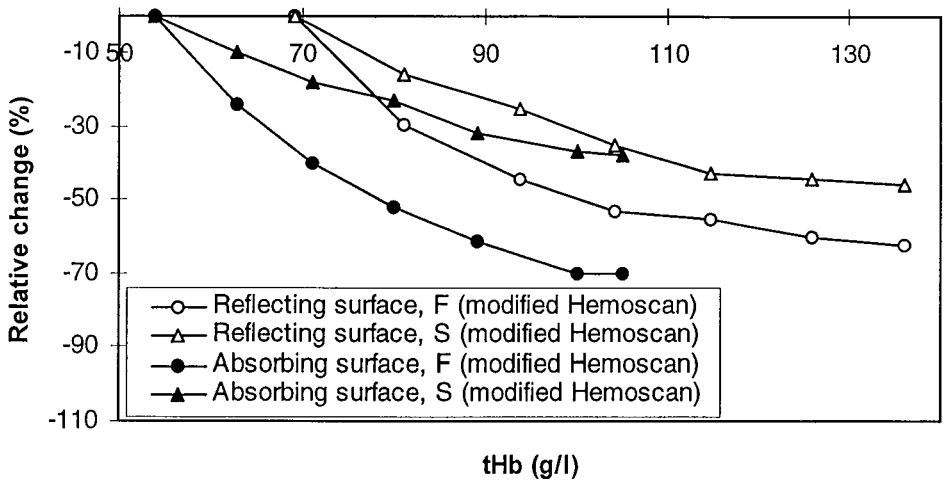

Figure 4.11 *The relative change in the side (S) and forward (F) scattering intensities are shown versus the total hemoglobin concentration, measured with an absorbing (whole blood with a hematocrit of 32.6% and an oxygen saturation between 45 and 55%) and a reflective geometry (whole blood with a hematocrit of 41.7% and an oxygen saturation between 30 and 40%). All standard deviations are within the range of the symbols.*

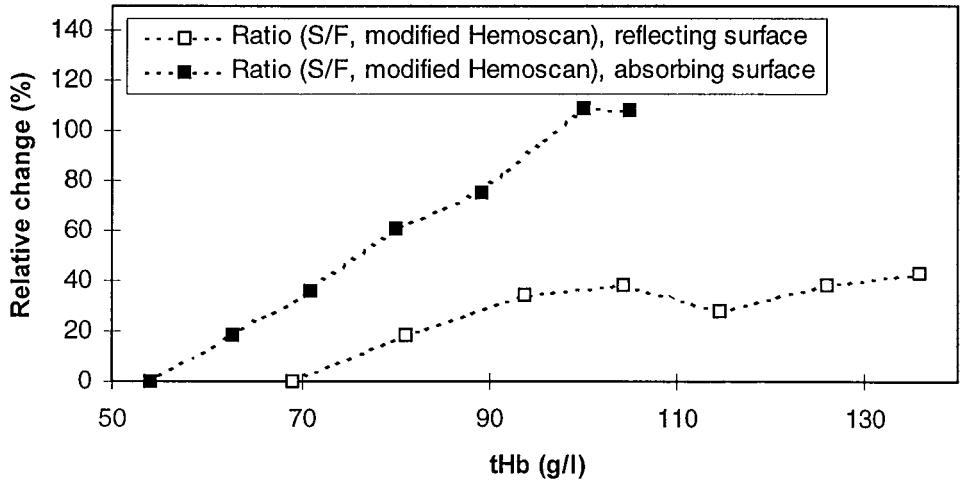

Figure 4.12 *The change in the ratio between the side (S) and forward (F) scattering signals, shown in Figure 4.11, relative the initial value of the ratio, is plotted versus the total hemoglobin concentration. The measurement was performed with an absorbing (whole blood with a hematocrit of 32.6% and an oxygen saturation between 45 and 55%) as well as a reflecting cavity surface (whole blood with a hematocrit of 41.7% and an oxygen saturation between 30 and 40%). All standard deviations are within the range of the symbols.*

4.1.4 Optical properties of the sample

The influence of the optical properties of the sample was investigated by performing extensive measurement series on latex/ink suspensions. The experimental results are shown in Figure 4.13 and Figure 4.14. It is clearly seen in Figure 4.13 that the surface has an exponential decrease both for the variation of the effective scattering coefficient and the absorption coefficient. Further, the surface in Figure 4.14 shows a rather smooth surface, except for the fourth absorption series. It is an average between the third and fifth absorption series due to an unsuccessful measurement. The side scattering signal decreases, when the absorption coefficient is varied (see Figure 4.14), in contrast to the more complicated performance when the effective scattering coefficient is varied.

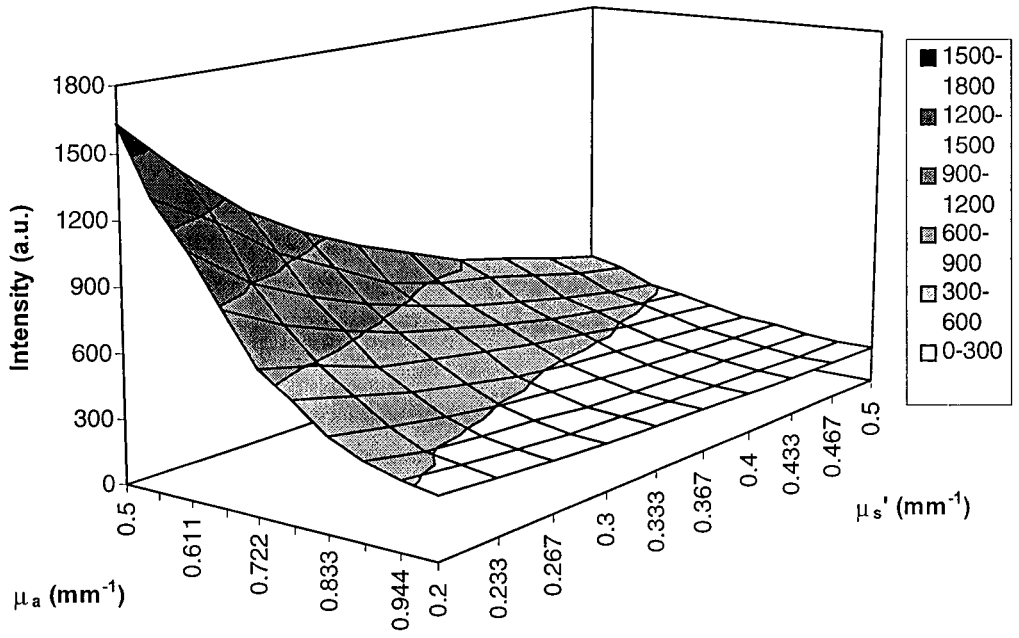

Figure 4.13 *Measured forward scattering intensity (arbitrary units) is plotted versus both the effective scattering coefficient* μ_s' *(from 0.2* mm^{-1} *to 0.5* mm^{-1} *in steps of 0.033* mm^{-1}*), and the absorption coefficient* μ_a *(from 0.5* mm^{-1} *to 1.0* mm^{-1} *in steps of 0.056* mm^{-1}*) of the latex/ink suspension. The g-factor was 0.9938*[25].

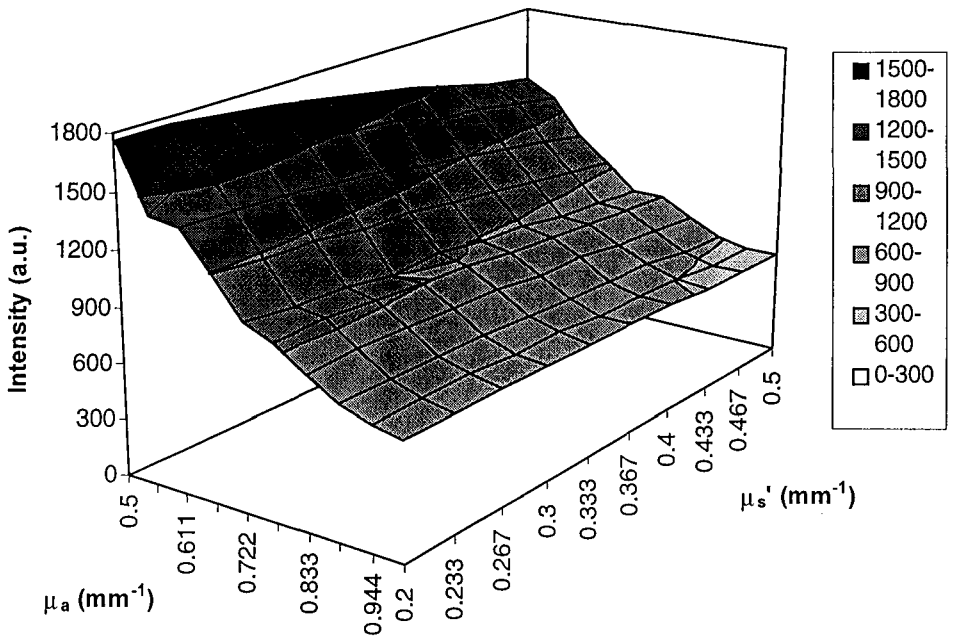

Figure 4.14 *Measured side scattering intensity (arbitrary units) versus both the effective scattering coefficient* μ_s' *(from 0.2* mm^{-1} *to 0.5* mm^{-1} *in steps of 0.033* mm^{-1}*), and the absorption coefficient* μ_a *(from 0.5* mm^{-1} *to 1.0* mm^{-1} *in steps of 0.056* mm^{-1}*) of the latex/ink suspension. The g-factor was 0.9938*[25].

In Figure 4.15, the measured ratio of the side to the forward scattering signals are compared to the ratio, obtained from the Monte Carlo simulations of a cylindrical cuvette geometry. The relative difference between the experimental and simulated results is calculated and shown in Figure 4.16.

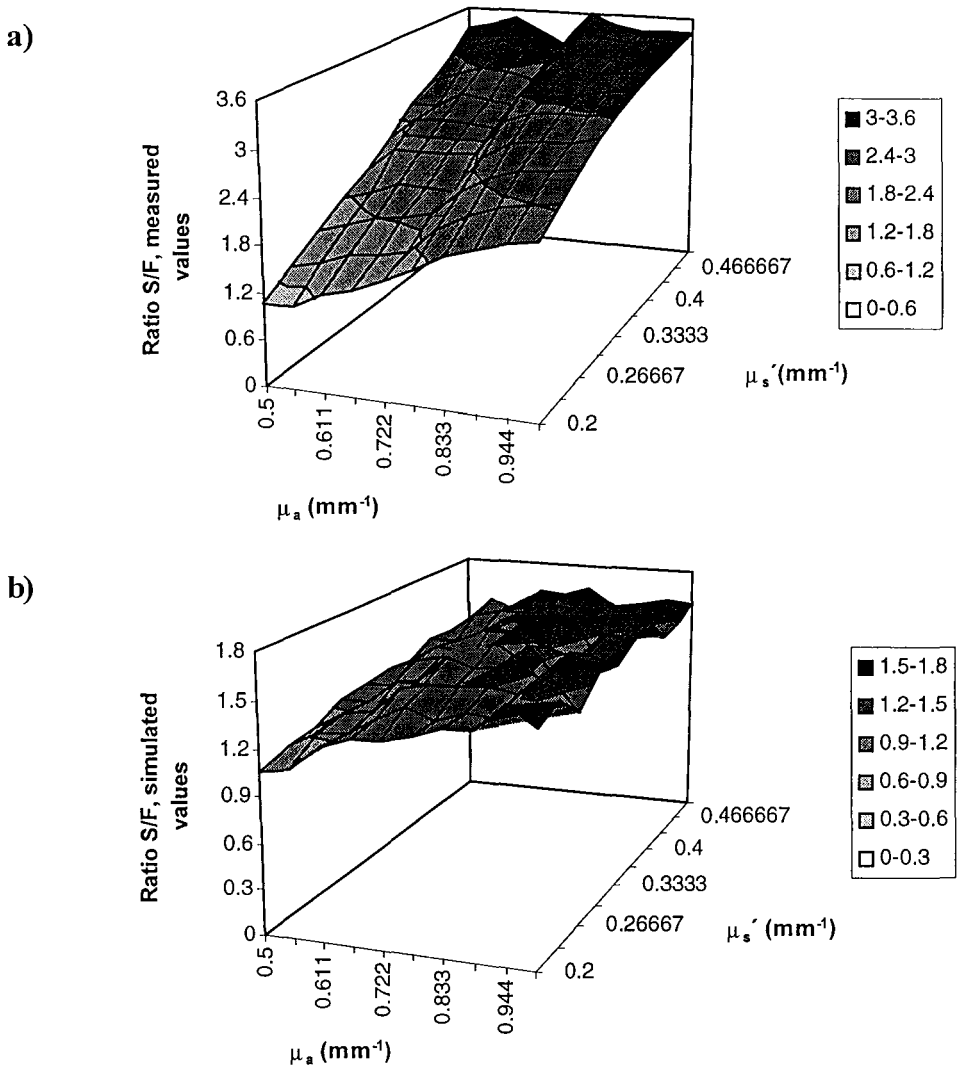

Figure 4.15 *The ratio of the side to the forward scattering signals are shown versus both the effective scattering coefficient μ_s' (from 0.2 mm^{-1} to 0.5 mm^{-1} in steps of 0.033 mm^{-1}), and the absorption coefficient μ_a (from 0.5 mm^{-1} to 1.0 mm^{-1} in steps of 0.056 mm^{-1}). In **a**), the ratios are taken from the measured values shown in Figure 4.13 and Figure 4.14, and in **b**), from Monte-Carlo simulated results.*

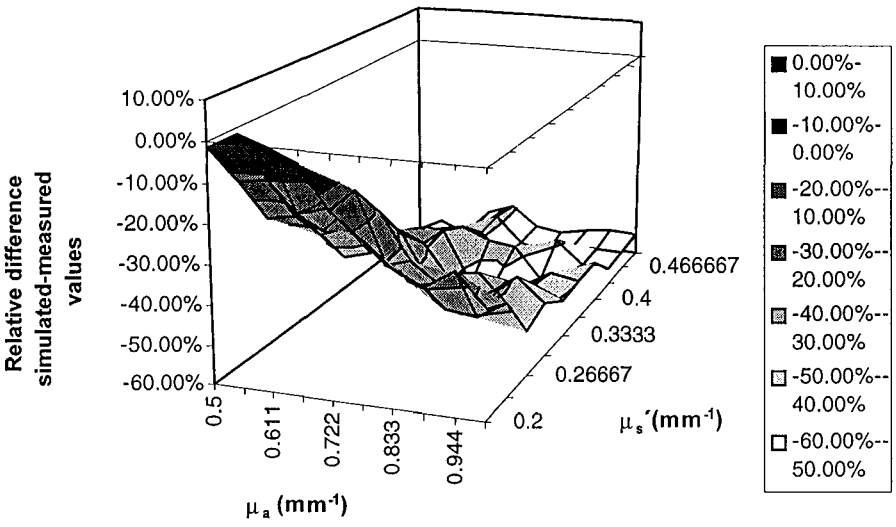

Figure 4.16 *The difference in simulated and measured ratios, relative to the measured are plotted versus the effective scattering coefficient* μ_s' *(from 0.2* mm^{-1} *to 0.5* mm^{-1} *in steps of 0.033* mm^{-1}*), and the absorption coefficient* μ_a *(from 0.5* mm^{-1} *to 1.0* mm^{-1} *in steps of 0.056* mm^{-1}*).*

The shape of the surfaces in the ratio diagrams (Figure 4.15 a-b) is similar, but the simulated ratio is flatter than that measured. In addition the absolute values differ; the measured ratio are significantly higher than those simulated. Figure 4.16 shows that the differences between the measured and the simulated ratio are great. A difference of more than 50% can be found for the combination of large absorption and scattering coefficients.

4.2 Simulated dialysis experiment

In the blood measurements the influence of several different parameters on the sensor signals were investigated. The response of the sensor to different arrangements as well as variations in total hemoglobin concentration, oxygen saturation, osmolarity and flow rate are presented in this chapter.

4.2.1 Optimisation of the experimental set-up

The influence and degree of hemolysis with the modified Hemoscan in a horizontal and vertical position, respectively, was investigated. In Figure 4.17 and Figure 4.18 a difference in forward and side scattering signals can be seen between the horizontal and vertical geometry. During the entire measurement the side scattering intensity for the vertical geometry is 3% lower than that for the horizontal geometry. The forward scattering intensity is only approximately 1% lower for the vertical geometry than that obtained with the horizontal arrangement in addition, this difference is within the standard deviations.

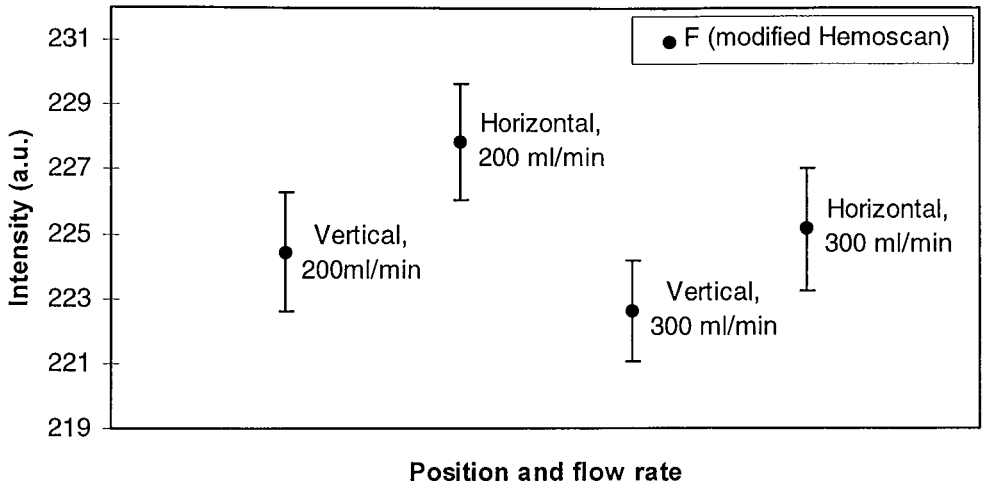

Figure 4.17 *Average values and standard deviations of the forward (F) scattering intensity are displayed, measured at the blood flow rates 200 ml/min and 300 ml/min, and with the sensor placed in a vertical (O_2sat=29%) and horizontal (O_2sat=27%) position, respectively. The hemoglobin concentration was 125 g/l.*

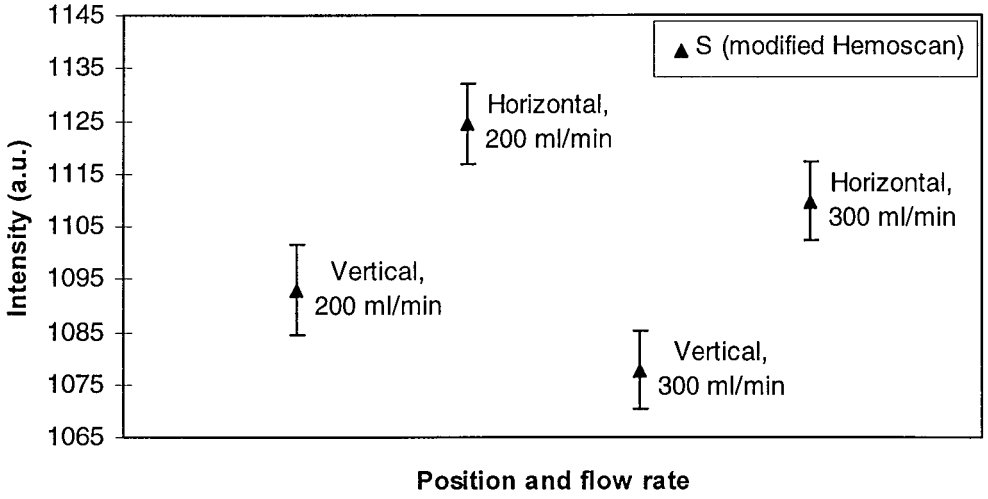

Figure 4.18 *Average values and standard deviations of the side (S) scattering intensity are shown, measured at the blood flow rates 200 ml/min and 300 ml/min, and with the sensor placed in a vertical (O_2sat=29%) and a horizontal (O_2sat=27%) position, respectively. The whole blood had a total hemoglobin concentration of 125 g/l (HCT=38.5%).*

When investigating the influence of a mini-oxygenator, three measurement series were performed. The first one lasted for one hour with one blood sample taken every tenth minute. The other two lasted for half an hour each and one blood sample was here taken every sixth minute.

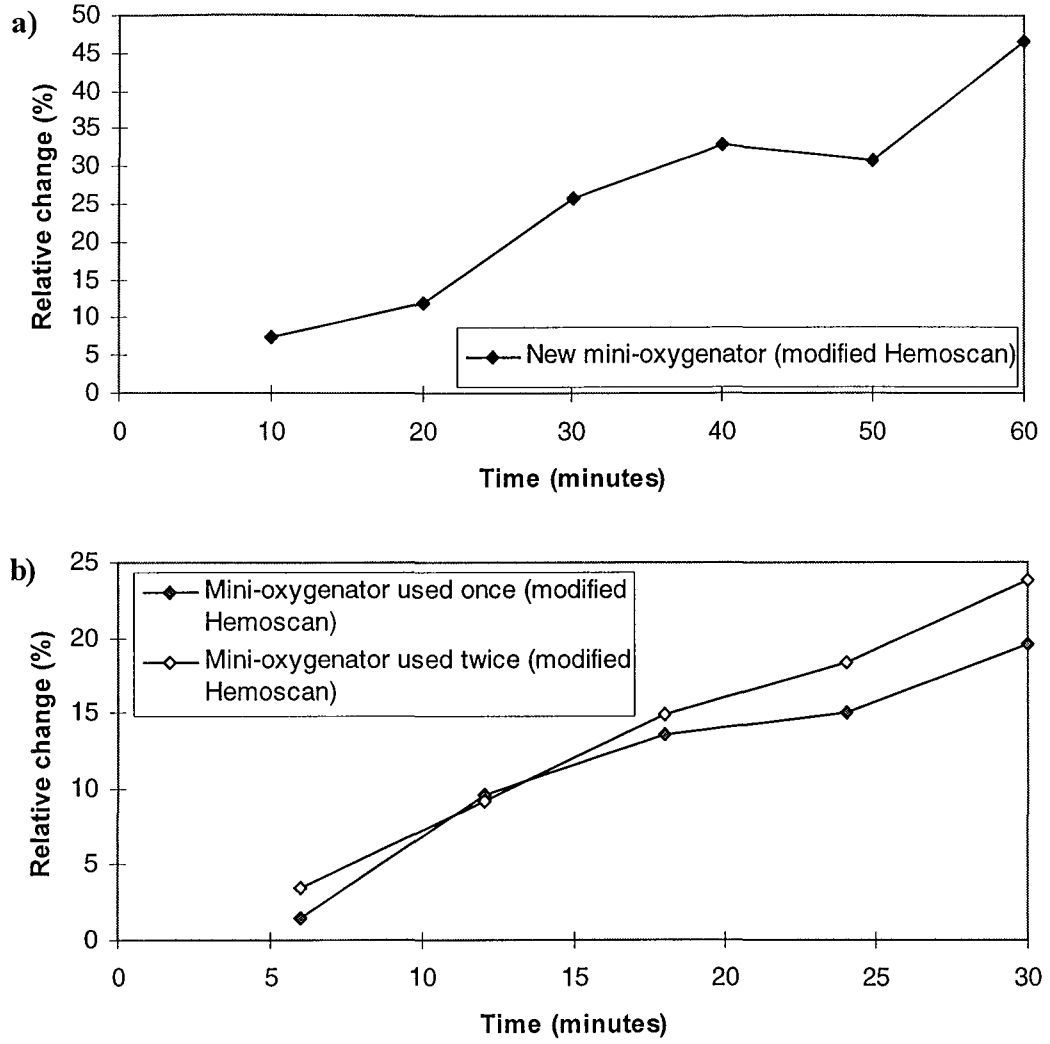

Figure 4.19 a-b *The relative change in the absorbance at 418 nm of centrifuged plasma are plotted versus time, during which the blood was pumped through a set-up with a new mini-oxygenator* ***a)*** *and a mini-oxygenator used once or twice* ***b).*** *The whole blood had a total hemoglobin concentration of 84 g/l (HCT=25%) and an oxygen saturation between 96 and 97%. The measurements where performed with a constant flow rate of 350 ml/min. All standard deviations are within the range of the symbols.*

It is shown in Figure 4.19 that the absorbance of centrifuged plasma increases approximately 25% during a measurement lasting for 30 minutes. In the first measurement (see Figure 4.19 a), the forward scattering signal decreased 12.0% and the side scattering signal decreased 7.4% when the absorption coefficient changed from 0 mm^{-1} to 0.16 mm^{-1}. In the other two experiments the corresponding decreases were 4.7 and 3.2%, respectively, when the absorption coefficient is changed from 0 mm^{-1} to 0.09 mm^{-1}. Thus, the decrease of the side scattering signal is less than for the forward scattering signal, if the absorption coefficient is increased. Furthermore, there are no obvious differences between the three experiments.

The influence of the connectors was investigated by using arrangements including different types of connectors.

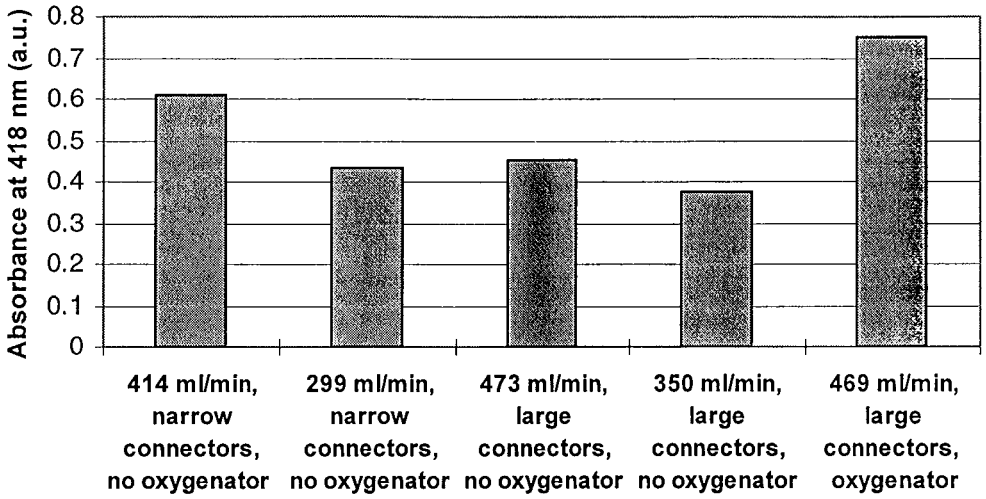

Figure 4.20 *The absorbance at 418 nm of centrifuged plasma after measurements using different kinds of arrangements. The narrow connectors have an inner diameter of 1.5 mm and the large connectors have the same inner diameter as the tubes (4.5 mm). The oxygen saturation varied between 18 and 25% for all the experiments, except for that employing a mini-oxygenator (97%). The total hemoglobin concentration was 111-114 g/l (HCT=35.3 %).*

In Figure 4.20 the maximum value of the absorbance spectrum is presented for different plasma samples. This value is taken at the wavelength 418 nm, i.e. the largest absorption peak of hemoglobin. It is shown that the absorption values are larger for narrow connectors than those for large connectors, even though the blood flow rates are lower. The largest absorption value is achieved when an oxygenator is used. However, it should not be compared with the other absorbance data, due to the high oxygen saturation associated with larger absorbance at 418 nm. When the absorbance increased, i.e. an increase of the degree of hemolysis, the decrease of the forward scattering signal is larger than for the side scattering signal, the same as mentioned in the previous section.

4.2.2 Hemoglobin experiments

The influence of the concentration of hemoglobin on the signals of the modified Hemoscan was investigated. Two measurements were performed, one with highly oxygenated blood versus one with less oxygenated.

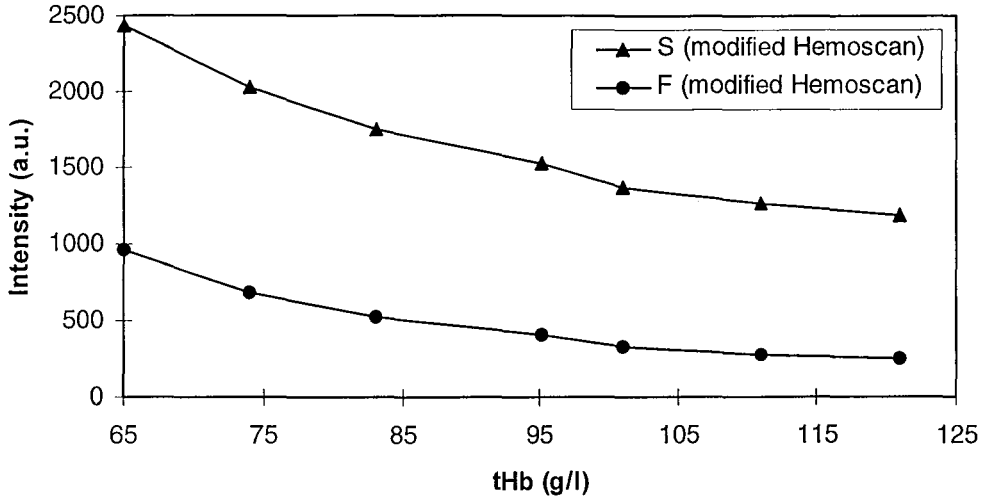

Figure 4.21 *The side (S) and forward (F) scattering intensities are plotted versus the total hemoglobin concentration. The whole blood had before being diluted a total hemoglobin concentration of 121 g/l (HCT=37.5%) and the oxygen saturation stayed at approximately 35%. The experiment was performed with a constant blood flow rate of 300 ml/min and a set-up without a mini-oxygenator. All standard deviations are within the range of the symbols.*

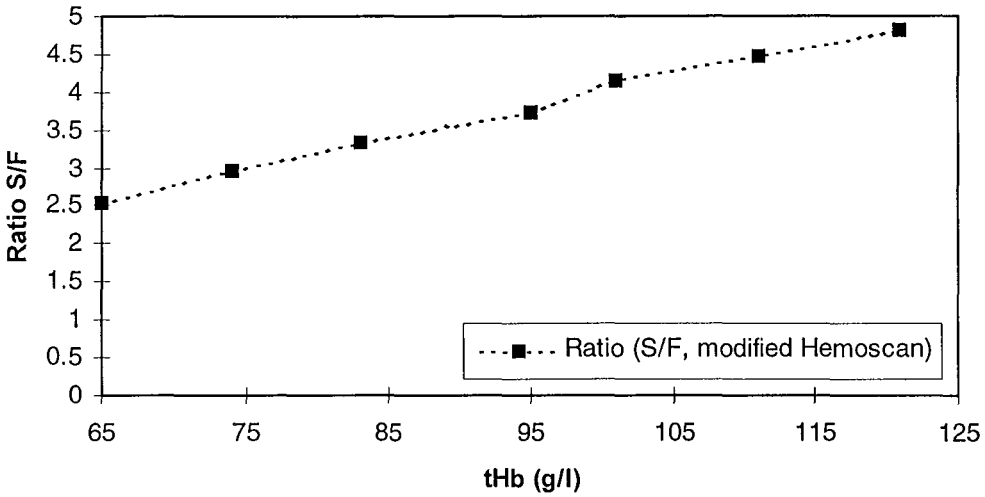

Figure 4.22 *The ratio between the side (S) and forward (F) scattering intensities is plotted versus the total hemoglobin concentration. The whole blood had initially a total hemoglobin concentration of 121 g/l (HCT=37.5 %) and the oxygen saturation was approximately at 35%. The experiment was performed with a constant blood flow rate of 300 ml/min and a set-up without a mini-oxygenator. All standard deviations are within the range of the symbols.*

The side and forward scattering intensities are both reduced with increasing concentration of total hemoglobin in blood, which can be seen in Figure 4.21. The ratio of the two signals is presented in Figure 4.22 and exhibits a linear increase of

approximately 90% when tHb is increased by 86%. The experiments were repeated using a mini-oxygenator in the set-up.

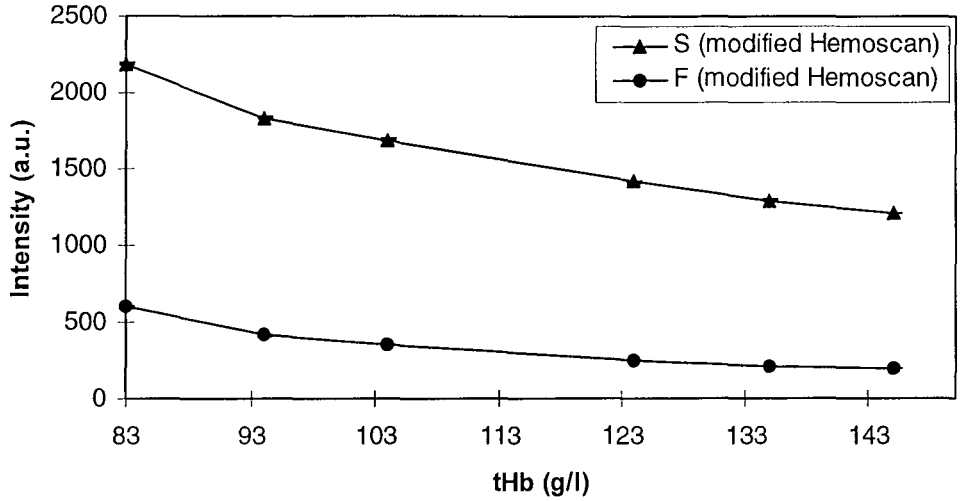

Figure 4.23 *The side (S) and forward (F) scattering intensities are displayed versus the total hemoglobin concentration, measured with an experimental arrangement including a mini-oxygenator. The whole blood had, before being diluted, a total hemoglobin concentration of 146 g/l (HCT=44.5 %) and the oxygen saturation stayed at approximately 96.4%. The experiment was performed with a constant blood flow rate of 300 ml/min. All standard deviations are within the range of the symbols.*

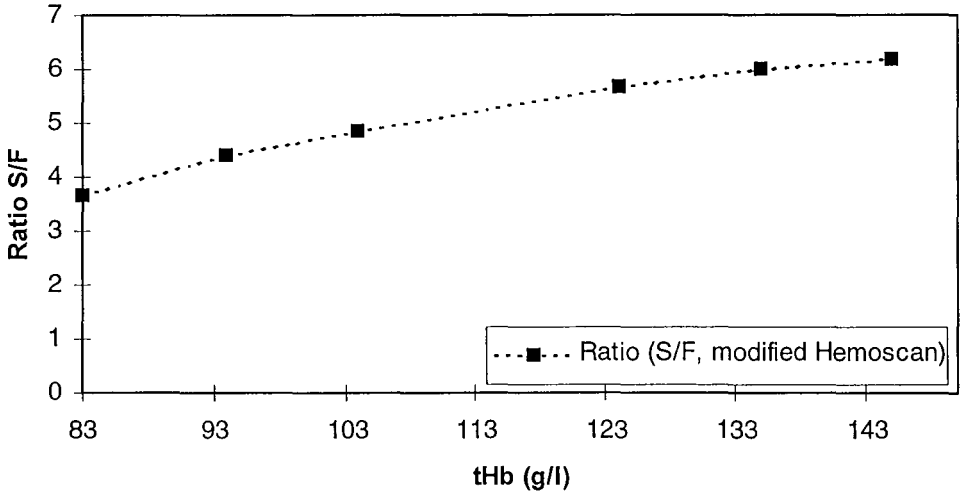

Figure 4.24 *The ratio between side (S) and forward (F) scattering signals is shown versus of the total hemoglobin concentration, obtained with an experimental arrangement using a mini-oxygenator. The whole blood had initially a total hemoglobin concentration of 146 g/l (HCT=44.5 %) and the oxygen saturation stayed at approximately 96.4%. The experiment was performed with a constant blood flow rate of 300 ml/min. All standard deviations are within the range of the symbols.*

The results presented in Figure 4.23 and Figure 4.24 was collected by using a set-up incorporating a mini-oxygenator. Again, the side and forward scattering intensities exhibit a decline with increasing concentration of hemoglobin. This results in an increase in the ratio (an increase by 70%, when tHb is increased 75%), however, not as linear as the ratio obtained from measurements performed without an oxygenator.

The set-up with the three sensors connected in series was used to investigate the performance of the sensors when the total hemoglobin concentration was varied.

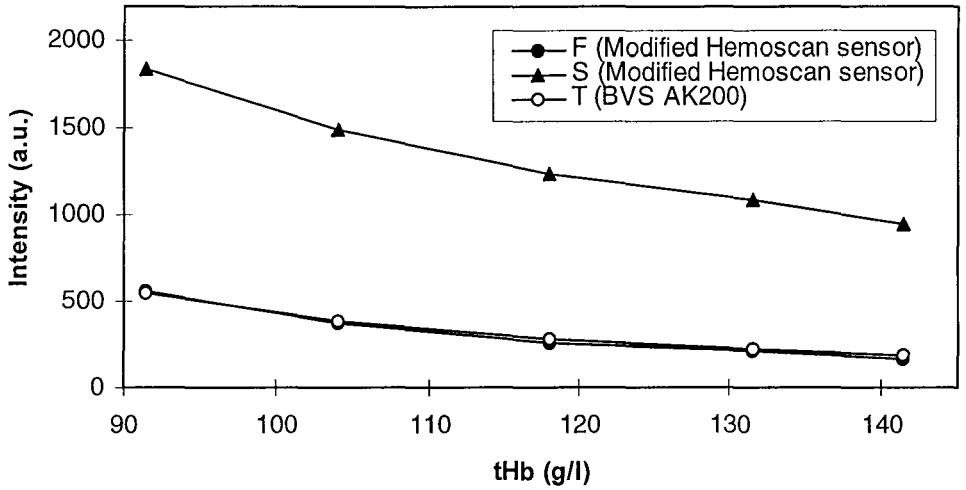

Figure 4.25 *The side (S) and forward (F) scattering intensities for the modified Hemoscan sensor in comparison with the transmitted (T) intensity for the BVS AK 200 are displayed versus the hemoglobin concentration. The total hemoglobin concentration of the whole blood before dilution was 141 g/l (HCT=40.9 %). All the blood samples had an oxygen saturation between 27 and 36%, except for the 18% obtained during the measurements on whole blood. All standard deviations are within the range of the symbols*

In Figure 4.25 it can be seen that the detected intensities for the modified Hemoscan sensor and the BVS AK 200 shows the same decreasing behaviour with increasing hemoglobin concentration. In addition, the absolute values of F and T coincide well.

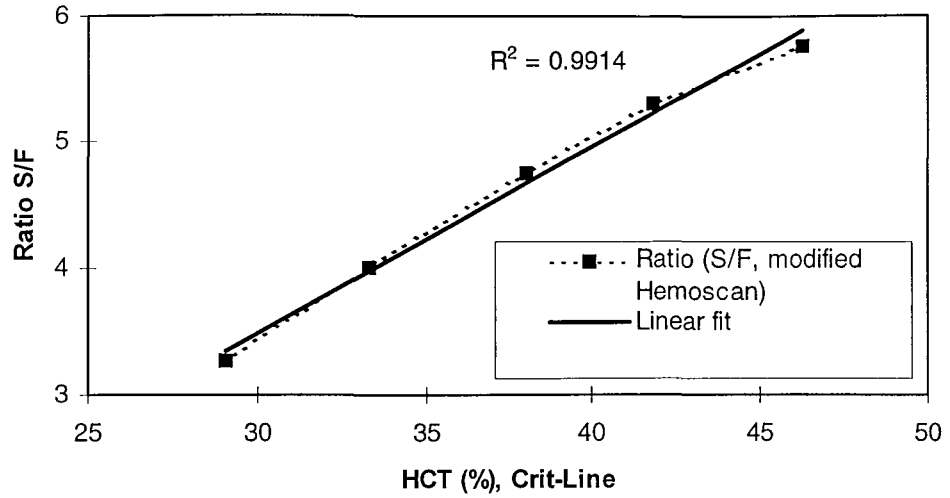

Figure 4.26 *The ratio of the side (S) to the forward (F) scattering intensities, obtained from the modified Hemoscan sensor, is plotted versus the hematocrit values given by the Crit-Line sensor. A linear fit is inserted with a correlation coefficient R^2=0.9914. The standard deviations are within the range of the symbols.*

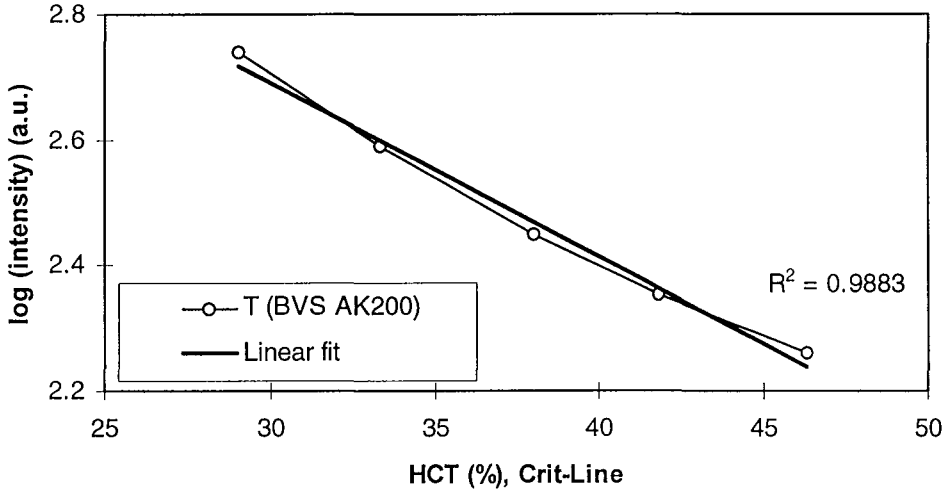

Figure 4.27 *The transmitted (T) intensity obtained from the BVS AK 200 is plotted versus the hematocrit values given by the Crit-Line sensor. A linear fit is inserted with a correlation coefficient of R^2=0.9883. All standard deviations are within the range of the symbols. All standard deviations are within the range of the symbols.*

The ratio (S/F) obtained from the modified Hemoscan sensor and the logarithm of the forward scattering intensity from the BVS AK 200, are displayed versus the hematocrit values collected by the Crit-Line along with the other two sensors in Figure 4.26 and Figure 4.27, respectively. The results of the modified Hemoscan sensor exhibit an almost linear dependence to the results of the Crit-Line sensor (the correlation coefficient is 0.9914). When the data representing the highest hemoglobin concentration is excluded (degree of oxygenation lower than for the other measurements), the correlation coefficient is even higher, i.e. 0.9993. The results of

AK 200 also show a similar relationship to the results of the Crit-Line sensor. However, when studying Figure 4.27 there seems to be a slight deviation from the linear behaviour. The correlation coefficient of the linear fit is lower, i.e. 0.9883 (0.9952 when the last data point is excluded).

4.2.3 Oxygen saturation experiment

When investigating the influence of the oxygenation of the blood, a mini-oxygenator was placed after a drip chamber with a filter, and they in turn were placed after the roller pump. A blood sample was taken every second minute.

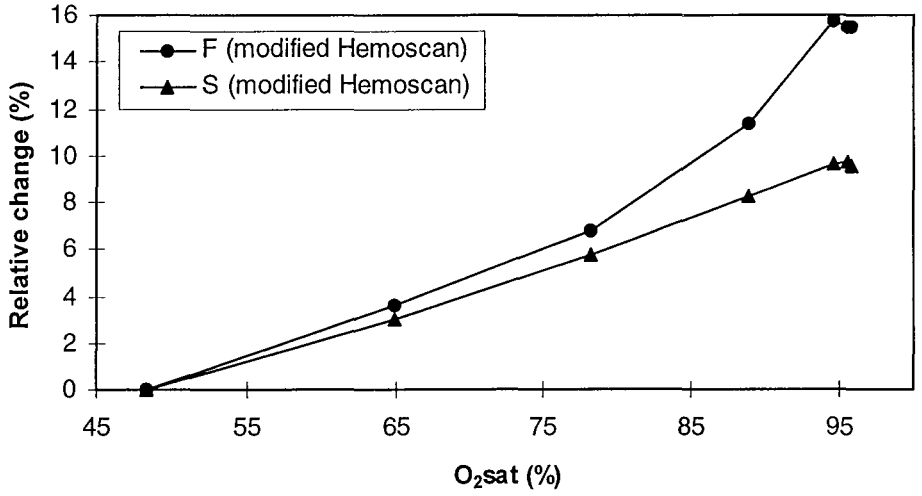

Figure 4.28 *The relative change in the side (S) and forward (F) scattering intensities are shown versus oxygen saturation of the blood. The whole blood had a total hemoglobin concentration of 127 g/l (HCT=39%) and was pumped at a flow rate of 300 ml/min. All standard deviations are within the range of the symbols.*

Figure 4.28 reveals that both the side and forward scattering signals are increased with increasing degree of oxygenation. It can be noted that the oxygen saturation of blood influences the forward scattering intensity more than the side scattering intensity. The former was increased by 15.5% and the latter increased by 9.6%, when the oxygen saturation was increased from 48.4 to 95.9%.

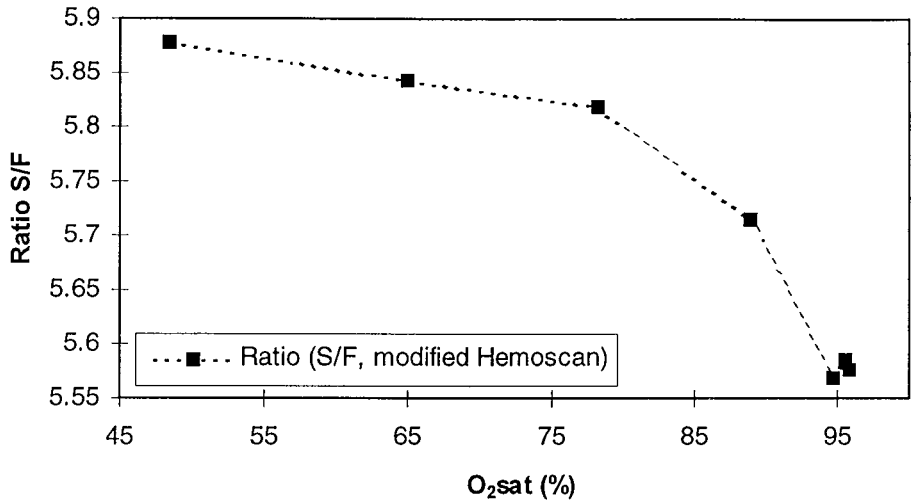

Figure 4.29 *The ratio between the side (S) and forward (F) scattering intensities are plotted versus the oxygen saturation of the blood. The whole blood had a total hemoglobin concentration of 127 g/l (HCT=39%) and was pumped at a flow rate of 300 ml/min. All standard deviations are within the range of the symbols.*

The ratio (see Figure 4.29) between the side and forward scattering intensities was in this experiment decreased by 5.1% when the oxygen saturation increased from 48.4 to 95.9%. However the decrease occurred mainly at saturation values higher than approximately 80%.

4.2.4 Osmolarity experiments

In order to investigate the influence of variations in osmolarity, the modified Hemoscan sensor measured on blood originating from five beakers of blood with different concentrations of NaCl solutions.

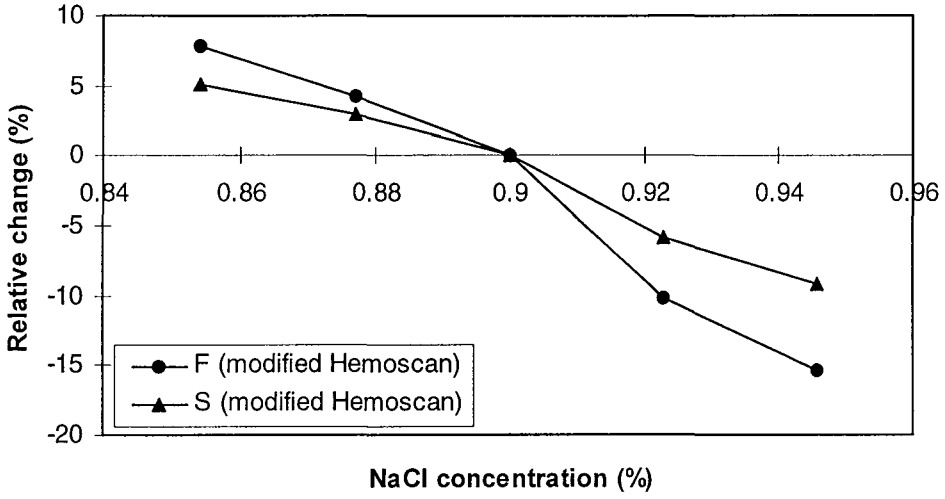

Figure 4.30 *The relative change in the side (S) and forward (F) scattering intensities are displayed versus the NaCl concentration in blood. The total hemoglobin concentration was for all samples 99 g/l (HCT=30%). The standard deviations are within the range of the symbols.*

In Figure 4.30 we can observe that the forward as well as the side scattering signals are reduced with increasing NaCl concentration. Furthermore, the forward scattering intensity is more affected by the osmolarity than the side scattering intensity. The intensity values are displayed relative the intensity obtained for the physiological value of the NaCl concentration in blood, i.e. 0.9%. The forward scattering intensity was reduced by 15.4% when the NaCl concentration was increased from 0.9 to 0.95%, whereas the side scattering intensity was reduced by 9.2%.

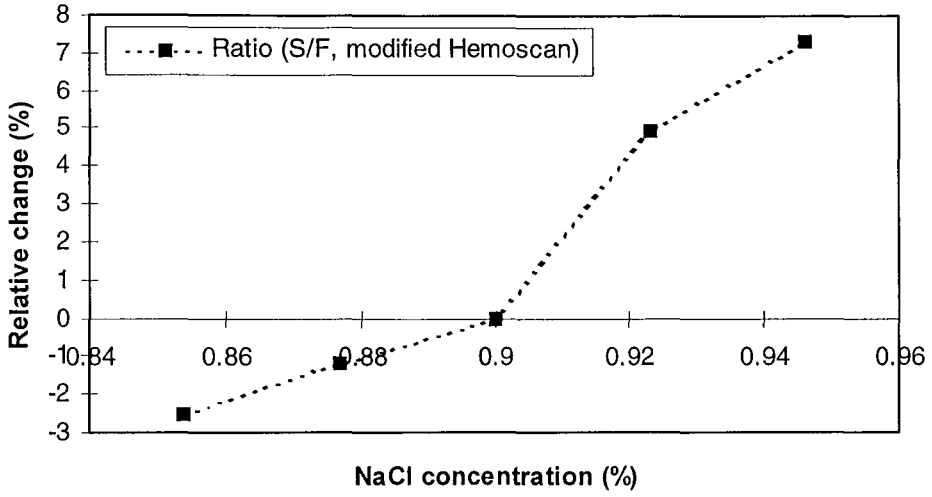

Figure 4.31 *The relative change in the ratio of the side (S) and forward (F) scattering intensities is plotted versus the NaCl concentration in blood. The whole blood is for all samples diluted to a total hemoglobin concentration of 99 g/l (HCT=30%). All standard deviations are within the range of the symbols.*

The relative change in the ratios of the two intensities is presented in Figure 4.31, showing an increase with increasing NaCl concentration. When the NaCl concentration was increased from 0.9 to 0.95%, the ratio was increased by 7.3%. It is interesting to note that the slope of the curve at sodium chloride concentrations lower than the physiological value differs from that at higher concentrations.

The response of the modified Hemoscan to variations in osmolarity of blood was compared to that of the BVS AK 200 and the Crit-Line.

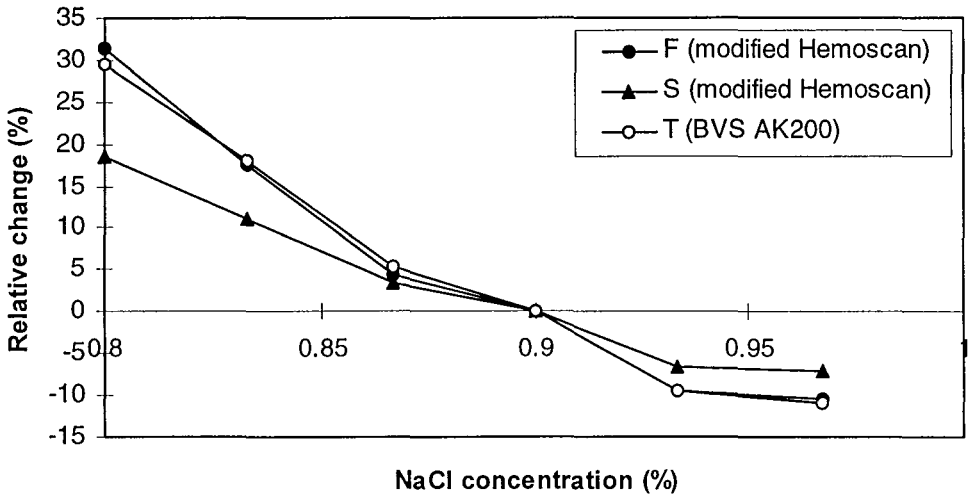

Figure 4.32 *The relative change in the side (S) and forward (F) scattering intensities for the modified Hemoscan sensor as well as the transmitted (T) intensity registered by the BVS AK 200, are displayed versus the NaCl concentration. The blood had initially a hematocrit of 40.9% and was diluted to 30% (tHb=103 g/l). The oxygen saturation was 22-24%. All standard deviations are within the range of the symbols.*

In Figure 4.32 it is shown that the forward scattering intensity changes in the same manner for the modified Hemoscan sensor as the transmitted intensity for the BVS AK 200. As previously seen (Figure 4.31), changes in osmolarity have a larger impact on the forward than on the side scattering intensity.

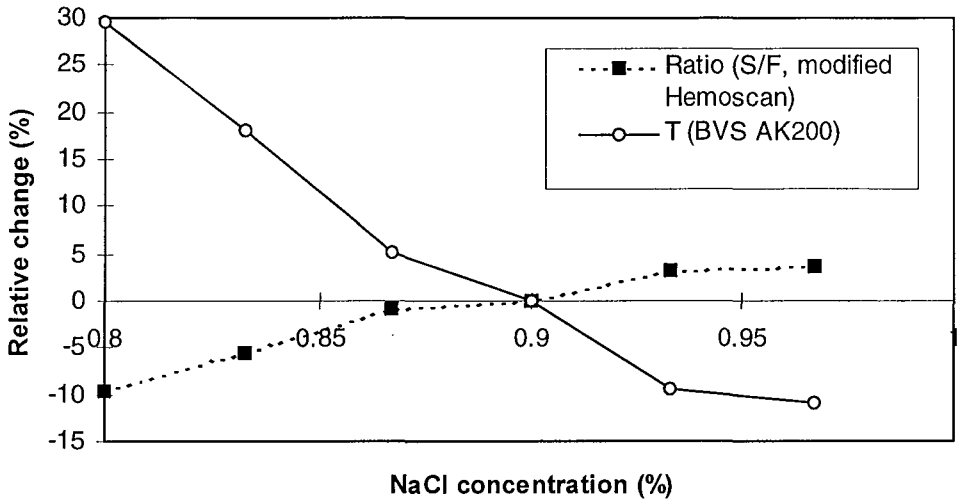

Figure 4.33 *The relative change in the ratio of the side (S) and forward (F) scattering intensities for the modified Hemoscan sensor is plotted versus the NaCl concentration, in comparison with the relative change of the transmitted (T) intensity for the BVS AK 200. The blood had initially a hematocrit of 40.9% and was diluted to 30% (tHb=103 g/l). The oxygen saturation was 22-24%. The standard deviations are within the range of the symbols.*

The relative change in the ratios of the side to the forward scattering intensity from the modified Hemoscan sensor is plotted in Figure 4.33 in comparison with that of the transmitted intensity recorded by the BVS AK 200. The impact of changes in osmolarity on the ratio is not as large as on the BVS AK 200 transmission signal. For the sodium chloride concentrations shown in Figure 4.33 the relative change in the ratio varies from -10 to 4% in comparison to from 30 to -10% for the BVS AK 200.

4.2.5 Flow rate experiments

The influence of changes in blood flow rate on the signals recorded by the modified Hemoscan was investigated.

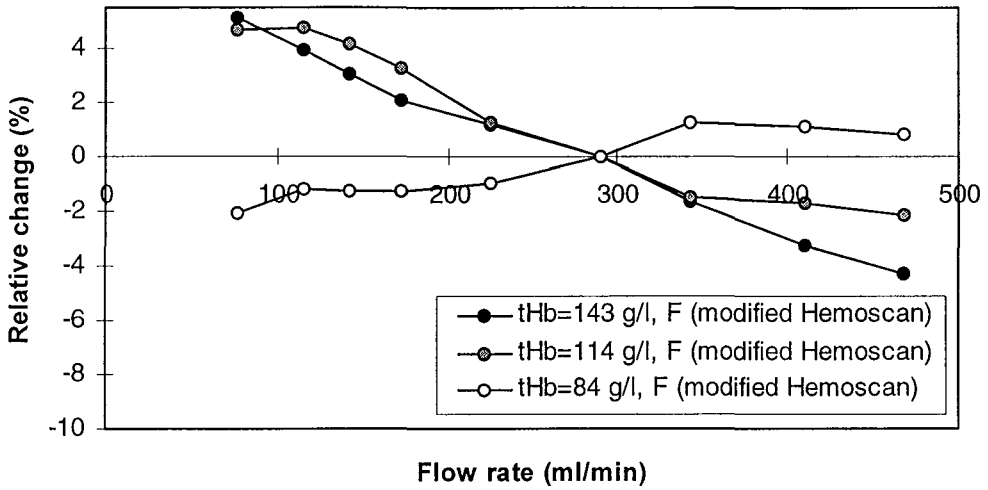

Figure 4.34 *The relative change in the forward (F) scattering intensity is shown versus the flow rate for different concentrations of blood. The oxygen saturation was 35% (tHb=84 g/l), 31% (tHb=114 g/l) and 18% (tHb=143 g/l), respectively. All standard deviations are within the range of the symbols.*

Figure 4.34 reveals the complex relationship between the forward scattering signal and the blood flow rate, as well as the concentration of hemoglobin. The intensity values are here plotted relative the forward scattering intensity obtained at a flow rate of 290 ml/min. The largest impact of the flow rate on the recorded signal can be seen for the blood sample with the largest hemoglobin concentration (tHb=143 g/l). The relative change varies from 5.1 to -4.3% in the flow rate range shown in the diagram. The influence of the flow rate at lower tHb concentrations is not as significant. It is thus interesting to note how the slope of the flow rate curves varies with the hemoglobin concentration; negative values at larger concentrations and positive at lower concentrations.

The general trend of the shape and slopes of the blood flow curves for the side scattering intensities (see Figure 4.35) is similar to that of the forward scattering intensities. The relative change varies at most from 3.1 to -5.0% for the sample with the largest hemoglobin concentration.

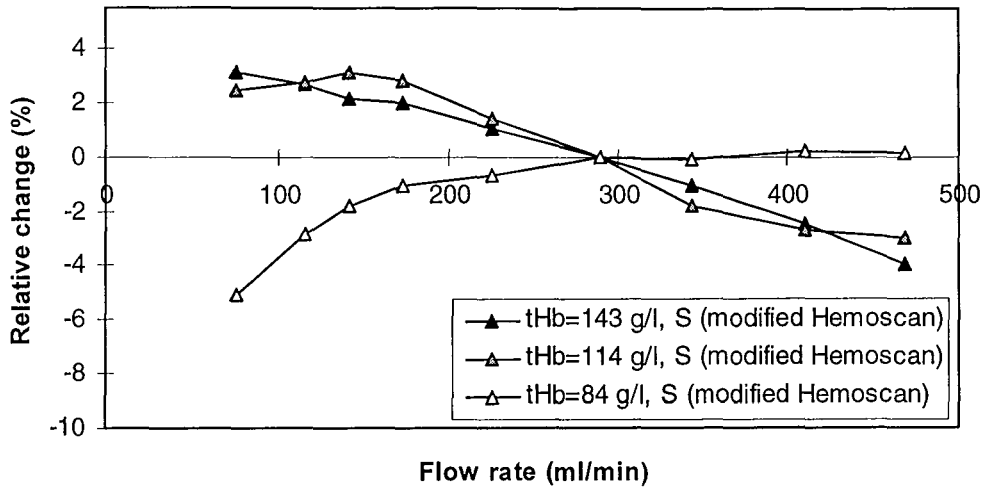

Figure 4.35 *The relative change in the side (S) scattering intensity is plotted versus the flow rate for different concentrations of hemoglobin. The oxygen saturation was 35% (tHb=84 g/l), 31% (tHb=114 g/l) and 18% (tHb=143 g/l), respectively. All standard deviations are within the range of the symbols.*

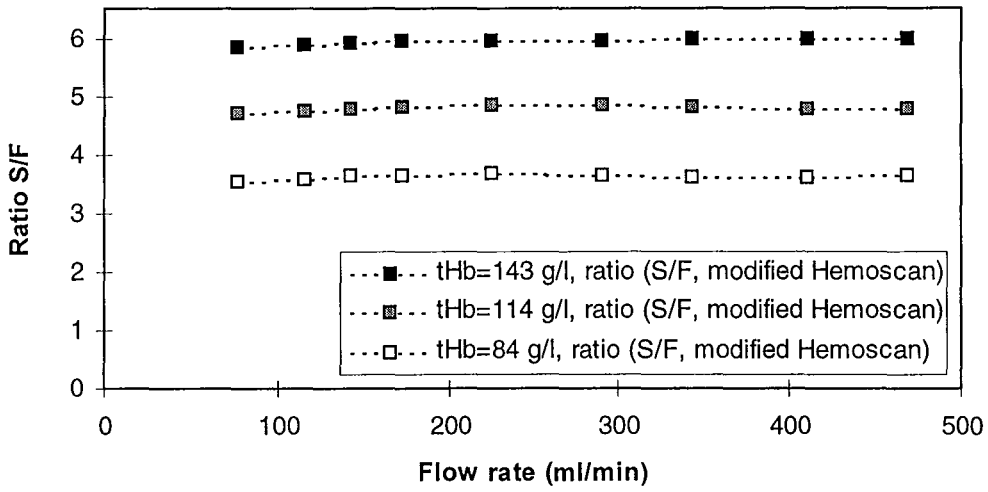

Figure 4.36 *The ratio of the previously displayed side (S) to the forward (F) scattering intensity is plotted versus the flow rate obtained for different concentrations of hemoglobin. Physiological NaCl solution (0.9%) was used for the dilution. All standard deviations are within the range of the symbols.*

Despite the differences in the slopes of the side and forward scattering intensity curves for different hemoglobin concentrations, the shape of the ratio curves looks similar, independent of the hemoglobin concentration (see Figure 4.36). It is also interesting to note that there are equivalent distances between the absolute values of the ratio curves, as a result of the different hemoglobin concentrations.

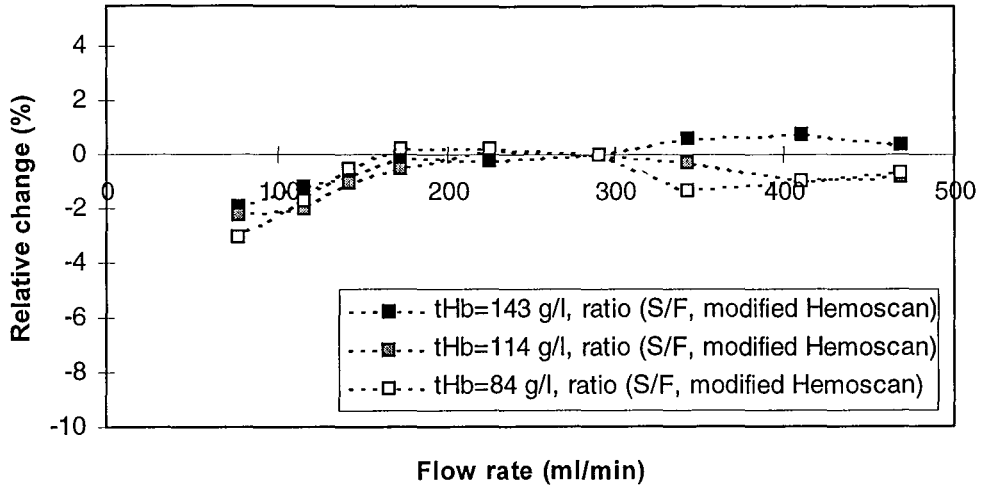

Figure 4.37 *The relative change in the ratios (S/F) for different concentrations of hemoglobin, are plotted versus the blood flow rate. The standard deviations are within the range of the symbols.*

The significant flow rate dependence seen for the forward and side scattering signals (Figure 4.34 and Figure 4.35) is reduced when forming a ratio. Figure 4.37 shows the flow dependent deviation of the ratios relative to the ratio obtained at 290 ml/min. For the flow rates below 290 ml/min, the relative change is in the order of 2-3% in the flow range shown in Figure 4.37. The corresponding value is 0.5-1% for the upper flow rate range.

The flow rate dependence was also investigated in a comparative study, which beside the modified Hemoscan included the BVS AK 200 and the Crit-Line. Figure 4.38 presents the signals recorded by the modified Hemoscan and the BVS AK 200 versus the blood flow rate. The curves are grouped with respect to the hemoglobin concentration. Again, the influence of the blood flow rate is most apparent for low flow rates (25 ml/min-150 ml/min), with a deviation in the order of 4-10% relative to the signal obtained at the flow rate 308 ml/min. It can also be seen that the shape of the curves depends on the hemoglobin concentration. At high concentrations the slope of the curve (disregarding the low flow rate range, 25-150 ml/min) is negative, becoming larger and even positive for lower concentrations. The ratio of the side to the forward scattering intensity depends on the flow rate as well, but not as much as the other signals do; in the order of 2 %. In
Figure 4.39, the standard deviations of the signals evaluated over the entire flow rate range are plotted for all three sensors, as a measure of the flow dependent variability. It can be seen that the ratio obtained from the modified Hemoscan and the hematocrit given by the Crit-Line have the smallest standard deviations in comparison to the other signals. It is important to note that the standard deviations of the hematocrit given by the Crit-Line are plotted in the same figure as the standard deviations for the other sensor intensities, despite that a direct comparison between these different units is not fully correct. The data from the Crit-Line is namely mathematically treated in order to give a hematocrit value, in contrast to the data from the other sensors that are displayed as the detected intensity. The standard deviations from the Crit-Line should thus be treated with care.

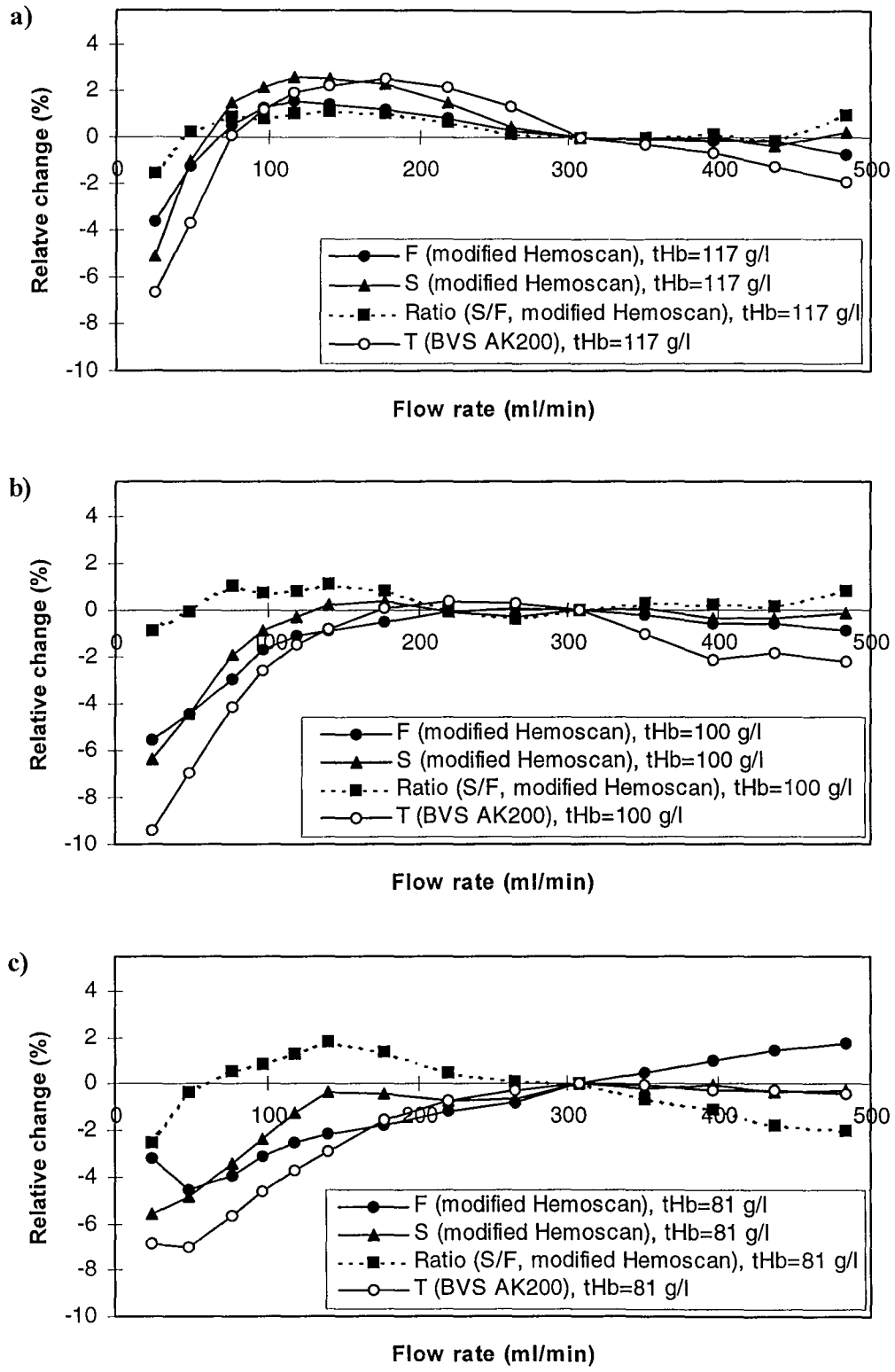

Figure 4.38 a-c *In this figure a comparison is made between the forward (F) and side (S) scattering intensities obtained from the modified Hemoscan sensor and the transmitted (T) intensity registered by the BVS AK 200, when the flow rate was varied. The total hemoglobin concentration was* ***a)*** *117 g/l (HCT=37.5%, O_2sat=32%),* ***b)*** *100 g/l (HCT=31.3%, O_2sat=43%) and finally* ***c)*** *81 g/l (HCT=25%, O_2sat=42%).*

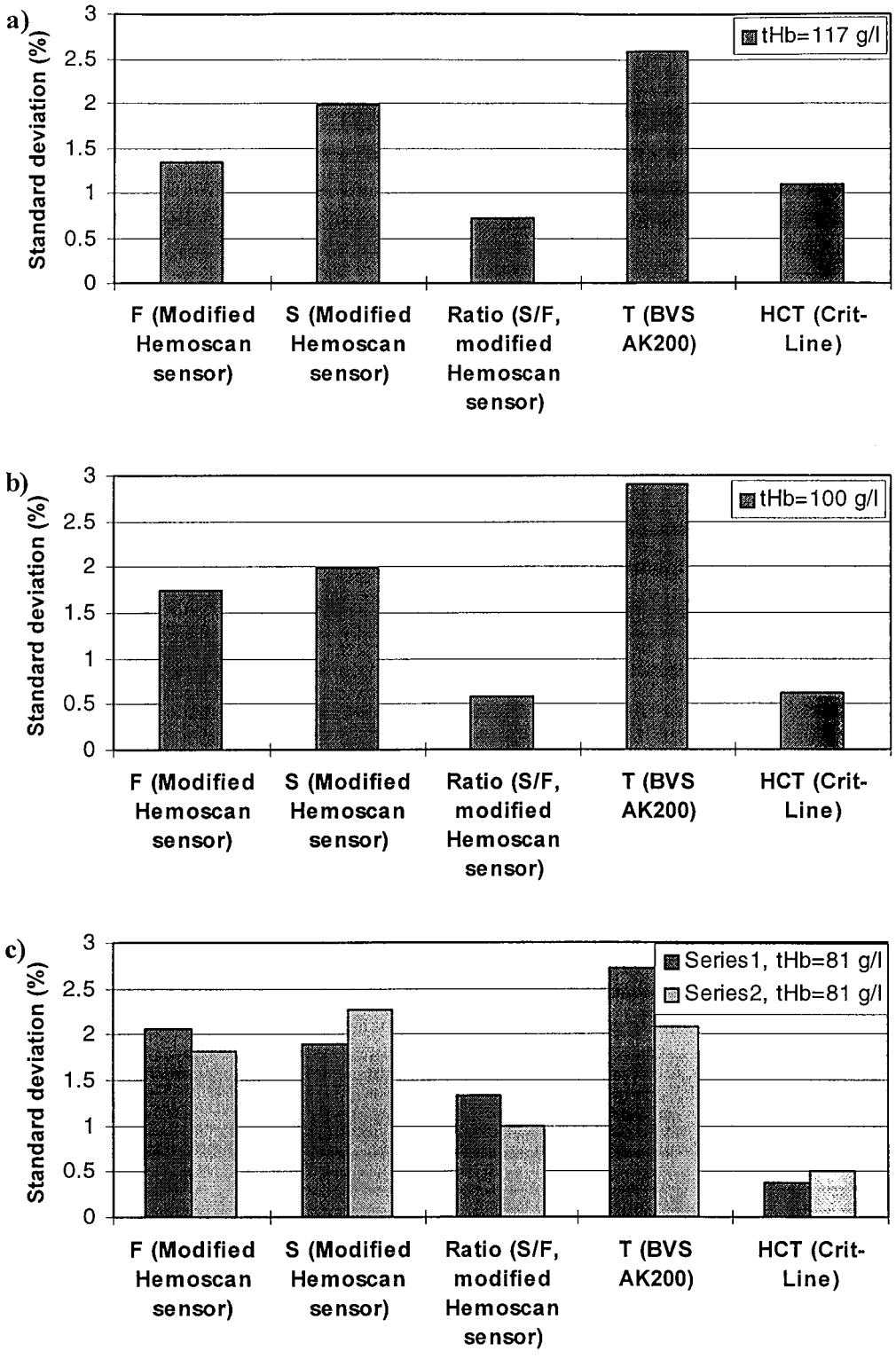

Figure 4.39 a-c *The standard deviations of the signals obtained from the modified Hemoscan, BVS AK 200 and the Crit-Line are displayed, expressed relative to the mean values when varying the flow rates between 25-483 ml/min. The hemoglobin concentration was* ***a)*** *117 g/l (HCT=37.5%, O_2sat=32%),* ***b)*** *100 g/l (HCT=31.3%, O_2sat=43%) and finally* ***c)*** *81 g/l (HCT=25%, O_2sat=43%). In* ***c)*** *two measurement*

series with blood from different batches (HCT=37.5% in series 1 and HCT=31.3% in series 2 before dilution to 25%).

Presenting the ratios, deduced from the signals of the modified Hemoscan, in the same manner as for the initial measurement series in Figure 4.36, the proportionality of the ratio to the concentration of hemoglobin is indicated (see Figure 4.40). The small flow dependent variations in the ratio can be seen here as well

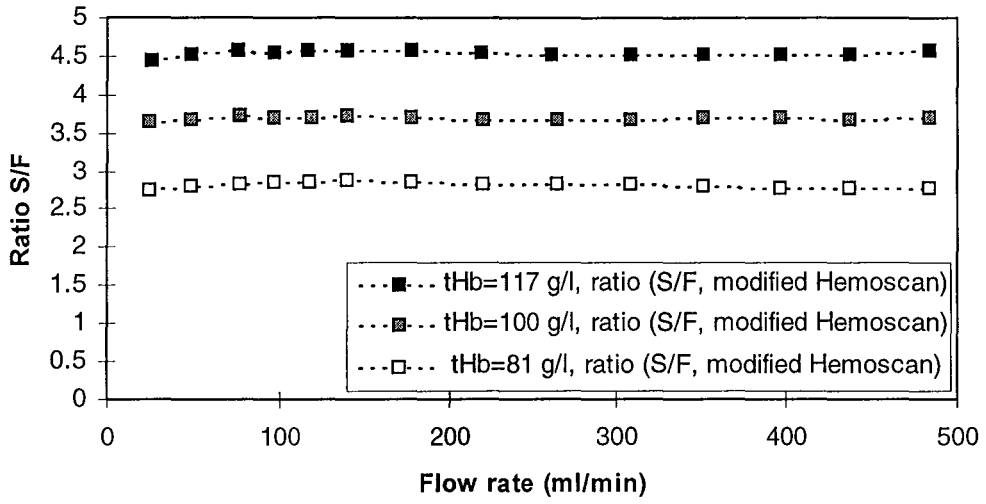

Figure 4.40 *The ratio of the side (S) to the forward (F) scattering intensity for different concentrations of hemoglobin are plotted versus the flow rate. The blood was here diluted with plasma in order to reach lower concentrations. All standard deviations are within the range of the symbols.*

Table 4.1 *A linear fit of the signals versus the flow rate in the range 177–308 ml/min for different concentrations of hemoglobin was performed. The slopes (k) and correlation factors (R^2) are shown in the table.*

	F (modified Hemoscan)		S (modified Hemoscan)		T (BVS AK 200)		
tHb (g/l)	$k*10^4$	R^2	$k*10^4$	R^2	$k*10^4$	R^2	Remark
117	-98	0.987	-182	0.975	-195	0.948	Batch 1
101	95	0.862	79	0.934	-47	0.735	Batch 2
100	36	0.621	-29*	0.384	-9*	0.095	Batch 1
91	1*	0.002	163	0.975	69	0.620	Batch 2
81	129	0.984	29*	0.273	119	0.938	Batch 1
81	133	0.996	206	0.953	91	0.834	Batch 2

*Unreliable data, due to low correlation coefficient.

A linear function was fitted to the data in the flow rate range 177-308 ml/min for six blood samples with different concentrations of hemoglobin. The slopes and correlation coefficients of these linear fits can be read in Table 4.1. It is worth noting that the measurements were performed for two different deliveries of whole blood (Batch 1: tHb=117 g/l, HCT 37.5% and Batch 2: tHb=101 g/l, HCT=31.3%). Neglecting the fits with low correlation coefficients (<0.5), there is a clear trend of

larger slopes with decreasing hemoglobin concentrations for the flow rate dependence of all three signals (F, S and T).

5. Discussion

The general purpose of this work, was to modify the original Hemoscan blood volume sensor, i.e. the BVS AK 200, in order to measure both the forward and side scattering light intensity, and evaluate if this modified sensor could monitor the relative change in blood volume with a higher accuracy. Several measurement series have been performed, varying different parameters of interest, and the recorded signals, as well as the ratio of them, were investigated and compared with the values given from other sensors.

5.1 Fundamental investigations of the sensor

Before investigating the influence of the blood and dialysis related parameters to the recorded detector signals, thorough studies were performed concerning the sensor cavity and the cuvette, using samples of latex and ink with well defined optical properties.

5.1.1 The cuvette

The task of the blood volume sensor is to monitor a slow change in concentration of blood cells during a dialysis treatment. Thus, in order to reproduce the received results, the stability of the measurement geometry is of high importance. The aim of the cuvette experiments described in section 3.1-2 and 4.1 was to investigate the influence of the position, and changes thereof, of the cuvette in the sensor cavity. Since the cuvette had an asymmetric shape, we found out that the detected signals were sensitive to variations in the placement of the cuvette into the sensor. Several long-term measurement series showed significant deviations from the initially recorded values when the cuvette was not properly placed in the sensor. If the cuvette was displaced 5 mm in sidelong direction, both the side and forward scattering intensities decreased by approximately 10 percent (see Figure 4.1). However, the ratio of the side to the forward scattering light did not deviate to the same extent; less than ±2 percent in the same range. When the cuvette was rotated 360 degrees, the forward scattering intensity varied about ±2% and the side scattering ±5% (see Figure 4.4). No improvement, in terms of less sensitivity, was gained by using the ratio S/F as evaluation parameter. It varied ±6% when the cuvette was rotated 360 degrees. The reasons to these variations are the slightly conical shape of the cuvette as well as that the central axes of the inner and outer cylindrical surfaces did not coincide. This indicates that the precision of the manufacturing of the cuvette is important and must be improved.

The recorded signals are also sensitive to damages to the cuvette. In order to avoid changes in the position of the cuvette in the cavity, the lid of the sensor must squeeze the cuvette tightly. If a sharp edge is in contact with the cuvette, scratches could then be formed on the surface. Experiments were performed with a small scratch made by a knife on the cuvette surface. The results showed that the impact on the signal was not

greater than that seen when rotating an undamaged cuvette. (Figure 4.5 and Figure 4.6). However, the sinusoidal dependence of the signals was lost for the damaged cuvette.

5.1.2 The sensor cavity

In order to investigate the influence of the optical properties of the inner surface of the sensor cavity, measurements were performed on a standard suspension both with a reflecting and an absorbing cavity surface. The standard suspension contained latex spheres and ink at various concentrations, which allowed us to vary the scattering and absorption properties of the sample in a controlled way. When the scattering coefficient was held constant and the absorption coefficient was varied, it was shown that the influence of the optical properties of the cavity surface was more significant for the forward scattering signal than for the side scattering. The same tendency followed when the absorption coefficient was held constant and the scattering coefficient was varied. Neglecting the intervals $\mu_a<0.6$ mm^{-1} and $\mu_s'<0.3$ mm^{-1} in Figure 4.7 and Figure 4.9, the side scattering signal appears to be independent of whether the cavity surface was reflecting or absorbing, whereas the forward scattering signal is lower for the absorbing cavity surface than for that reflecting. Consequently, the ratio of the side to the forward scattering intensity increased almost linearly with increasing absorption or scattering coefficients when using an absorbing sensor cavity, whereas it was more or less constant for the reflecting sensor cavity. (see Figure 4.8 and Figure 4.10). When blood was used, similar results were obtained. The side and forward scattering intensities were here plotted versus the total concentration of hemoglobin, tHb (g/l). Two series, varying tHb, were measured however, at different occasions. The blood was collected from two different blood batches and the tHb intervals were therefore not the same in the two measurement series. However, the trend of the ratio S/F for blood is the same as in the latex/ink suspension, i.e. a stronger dependence of the ratio on the tHb-value when measurements are performed using the absorbing cavity surface than that reflecting.

Our intention was to use the ratio S/F rather than the absolute values of S and F when constructing an algorithm to relate measured data to the parameter of interest, i.e. the relative blood volume. Since our results suggest that the ratio has a more linear and stronger dependence on the hemoglobin concentration when an absorbing sensor cavity is used, we adopted this cavity sensor for our experiments.

5.1.3 The light propagation

The purpose of this study was to investigate the response of the sensor to variations in both the absorption and the scattering coefficients, and then to compare them with Monte Carlo simulations. The reason for this is that Monte Carlo simulations give insight into the characteristics of the light propagation in the sample and cuvette. Input parameters to the simulation program were the optical properties of the blood and the cuvette as well as parameters defining the cylindrical sample and cuvette geometry being modelled. The absorption and scattering coefficients treated experimentally and by the simulations, were chosen after an extrapolation of the optical properties of

blood given at 633 nm to 800 nm and after comparison to measured values[16]. The fourth measured series (μ_a=0.667 mm^{-1}, 0.200 mm^{-1}<$\mu s'$<0.500 mm^{-1}) was erroneous and in Figure 4.13 and Figure 4.14, this series is replaced by mean values of the third and fifth series. The reason for this was probably the accuracy of the optical properties of the main solutions of latex and ink. In each series, two solutions were prepared with the same absorption properties but different scattering properties. By mixing them in various proportions, a series with increasing scattering coefficient but constant absorption coefficient was received. If the optical properties of the main solutions were erroneous, the recorded data from whole series would be shifted, which was the case in the fourth series.

Comparing Figure 4.15 and Figure 4.16 indicates that the measured and simulated values do not correspond particularly well. The relative difference in the simulated versus measured ratios increases with increasing absorption and the scattering coefficients, and is more than 50% in some cases. Since the cuvette geometry was shown to have such a large impact on the recorded signals, the same cuvette was used for all ten measurement series. A diffuse coating from the latex suspension was thus gradually formed on the inner surface of the cuvette which may cause measurement errors. This was also the reason for not measuring the fourth series again. However, this possible source of error could not fully explain the great differences between the measured and simulated results. It is more likely that the geometrical model of the sample and the light source used in the simulation program is not sufficient. The optical properties of the sensor cavity surface must be incorporated and the procedure treating the divergence of the light source must be further looked upon. In the simulation procedure, a photon that exits the PVC layer of the cuvette to the surrounding medium vanishes. In reality, there is always a certain amount of photons being reflected by the sensor cavity surface, even if it is painted black. This should be included in the model. Furthermore, the sensor has a short and narrow path guiding the light from the light source to the cuvette. This path is cylindrical with a diameter of 3.5 mm, and the surface is aluminium. When the divergent light from the LED passes through the cylinder, it can be reflected in the walls and the distribution of the incident light is therefore difficult to model accurately. In the simulations, the length of this cylinder was chosen to 3.4 mm but in the reality, it is 4.5 mm. The reason for this is the cylindrical LED cavity shown is Figure 3.1. The extra length, due to the LED cavity, was not taken into consideration in the simulations, which certainly affected the simulation results. A longer cylinder from the light source to the cuvette results in an increase of the ratio of the reflected photons in the aluminium surface to the total number of photons from the source. Thus, the light intensity decreases due to absorption in the aluminium surface, and the photons entering the cuvette will have a more complicated angular distribution.

5.2 Blood measurements

In this section, we will discuss the modified Hemoscan sensor response to variations in different blood and dialysis related parameters. Furthermore, a comparison of the modified to the original Hemoscan and a commercially available blood volume sensor (Crit-Line) will also be dicsussed.

5.2.1 Optimisation of experimental set-up

Different kinds of experimental arrangements were investigated in order to see how certain set-up related parameters influenced the measurements. When the sensor was placed in a horizontal and vertical position respectively (see Figure 4.17 and Figure 4.18), there was a slight difference in the recorded signals depending on the orientation of the cuvette. The side scattering signal was affected by the orientation to a larger extent than found for the forward scattering signal. This orientation dependence may be explained by differences in alignment and aggregation of red blood cells in the tubes when the measurements are performed in the two different geometries. The light scattering properties of blood are namely highly influenced by the size, shape and alignment of the cells[22]. Changes in these microscopic properties of blood will thus affect the side scattering signals. The fact that this was mainly observed for the side scattering signal, may indicate a stronger dependence on the scattering properties. However, in order to conclude this, simulations based on a realistic model are required.

In order to estimate the damage of red blood cells caused by critical components in the experimental set-up, the degree of hemolysis was measured by taking samples during long-term measurements. The samples were centrifuged and the degree of hemolysis was determined by measuring the amount of hemoglobin dissolved in the plasma[23]. Plasma does essentially not contain any hemoglobin when the red blood cells are undamaged. The critical components in the set-up, in viewpoint of hemolysis, were a mini-oxygenator and narrow tube connectors. The mini-oxygenator consists of hundreds of fibres, each with a diameter of 100 μm, which at high flow rates may cause damage to the red blood cells during passage. This is indicated by the significant decrease in hemoglobin absorbance of the plasma when using a flow set-up with a mini-oxygenator. Thus, the mini-oxygenator was only used for experiments where a high oxygen saturation of the blood was essential. The hemolysis rate seems also to be dependent on which kind of tube connectors that are used. The results presented in Figure 4.20 indicate that the hemolysis rate is larger when using the narrow connectors in the flow set-up than when using the connectors with large diameters, even if the flow rate was higher. The reason for this is most likely that the smaller diameter, 4 times less in the narrow connectors compared to the large ones, generates approximately a 16 times higher pressure and thus a higher risk for causing damage to the cells. A further observation was that a narrow connector created a more turbulent flow at high flow rates This in turn made a placement of a narrow connector near the sensor inappropriate. Large tube connectors were thus used in the flow set-up.

The primary characteristics of the recorded signals when hemolysis occurred was a slight, long-term decrease of both the side and forward scattering intensities while other parameters were held constant. The reason for this is the increasing amount of hemoglobin in the plasma, due to leakage from the membranes of the damaged red blood cells. The dependence of the relative change in the recorded signals and the increase in the absorption coefficient of the plasma was investigated. The tendency was always that the forward scattering signal decreased more than the side scattering. However, it is difficult to estimate a measure of the dependence since the plasma of the untreated blood contained various amounts of hemoglobin. Furthermore, a high

value of cell concentration could give such weak recorded signals that there is no longer a linear response of the detector. Therefore, a quantitative evaluation of this dependence is not appropriate.

It is also important to remember that there are several other factors in the flow set-up that continuously may affect the measurements. For example, it is known that the roller pump has a tendency to damage the red blood cells to a certain extent[23].

5.2.2 Hemoglobin experiments

In eq. (1.1) and (1.2), the dependence of changes in blood volume and changes in hemoglobin or hematocrit is given. The main condition for these formulas is that there is no bleeding during the dialysis treatment, i.e. the number of red blood cells remains constant. If the impact on the recorded signals due to hemolysis could be neglected, a measurement giving the relative change in hemoglobin concentration could be used to monitor the changes in blood volume. Thus, the hemoglobin experiments are essential in this work.

Decreasing side and forward scattering signals were found in Figure 4.21 with increasing total hemoglobin concentration. On the other hand the ratio (see Figure 4.22) increases with the hemoglobin concentration, which means that the decrease in the forward scattering signal is more significant than that in the side scattering signal. The decrease in the two signals with increasing amount of hemoglobin seems logical, since an increase in red cell concentration correspond to increasing absorption and scattering coefficients reducing the amount of light passing through the cuvette[22].

When the flow set-up included a mini-oxygenator in order to reach high O_2sat-values, the same appearance of the tHb dependence of the recorded signals was observed (see Figure 4.23). However, a slight divergence from the linear dependence of the ratio on the tHb-value was seen for larger concentrations (Figure 4.24). An explanation to this might be the influence of the mini-oxygenator, since it is suspected to hemolyse the blood (see 5.2.1), particularly at high cell concentrations. A more likely explanation might be, as previously mentioned, that one of the two signals (probably the forward scattering) turns too weak for a linear response of the photo diode at high hemoglobin concentrations. In the experiment using the mini-oxygenator, the maximum concentration of total hemoglobin was as high as 145 g/l in comparison to 121 g/l in the former experiment. The divergence from the linear dependence in the experiment on blood with high hematocrit occurred at a tHb-value of approximately 125 g/l.

In the hemoglobin experiment, including three different sensors, a comparison between the commercially available Crit-Line and the modified Hemoscan could be done. It turned out that there is a nice linear dependence between their output data, i.e. the monitored hematocrit value from Crit-Line and the ratio S/F of the modified Hemoscan (see Figure 4.26). The correlation coefficient of the linear fit was 0.9914. The last one of the five data points, i.e. from the measurement on the highest concentration of hemoglobin, seemed to deviate more from the liner fit that the other ones. This might be explained by the low value of the forward scattering signal at such high concentrations of hemoglobin. As previously mentioned, the linear response of

the photo diode could then be lost. When this data point is excluded, the correlation coefficient is as high as 0.9993. The dependence between the logarithm of the transmitted intensity from the BVS AK 200 and the hematocrit values from the Crit-Line is shown in Figure 4.27. It turned out to be less linear, with the correlation coefficient 0.9883 (0.9952 when not using the data obtained at the highest hemoglobin concentration). It seems as if the dependence rather constitutes a weak exponential behaviour.

Concerning the monitored values of the hematocrit from Crit-Line, it is not fully clear how to compare them with the measured intensities from the modified Hemoscan BVS and the BVS AK 200. According to the Beer-Lambert law (eq. 2.5), there is a logarithmic dependence between the transmittance I and the total interaction coefficient μ_t, i.e. $\log I \propto \mu_t$. Since the hematocrit, given by the Crit-Line is proportional to the amount of absorbers and scatterers in the blood, it can be assumed that the total interaction coefficient also is proportional to hematocrit. From this follows that $\log I \propto hct$. However, Crit-Line uses a vibrating membrane, which varies the sample thickness x. If the Beer-Lambert law is differentiated with respect to time, and then linearised by:

$$\frac{\partial}{\partial t} \rightarrow \frac{\Delta}{\Delta t}, \tag{5.1}$$

following expression can be derived:

$$\frac{\Delta I}{I} = -\mu_t \Delta x. \tag{5.2}$$

Crit-Line monitors the transmitted intensity at several different wavelengths (see Patent No. WO94/27495, Robert Steuer). When equation (5.2), formulated for one wavelength λ_1, is divided by that formulated for a second wavelength λ_2, the following expression is given:

$$\frac{(\Delta I/I)_{\lambda_1}}{(\Delta I/I)_{\lambda_2}} = \frac{\mu_t(\lambda_1)}{\mu_t(\lambda_2)}. \tag{5.3}$$

Thus, the output of the Crit-Line (hematocrit) is given by the measured intensity and its variation via a linearised exponential expression. However, Crit-Line's hematocrit is still proportional to the interaction coefficient. Since no linearised expression is applied to the intensities recorded by the modified Hemoscan and the BVS AK 200, a comparison between the logarithm of the intensities and Crit-Line's hematocrit should be the best method available, if just using one recorded signal. Still, the ratio S/F has the most linear dependence to the Crit-Line's hematocrit and in this case, there is no need for calculating the logarithm.

5.2.3 Oxygen saturation experiment

The experiments investigating the influence of oxygen saturation of blood on the optical signals show a clear dependence. The side and forward scattering signals both increased with increasing degree of oxygenation, mainly at saturation values higher than 80%. The largest impact was observed for the forward scattering signal. For this reason, the ratio between the signals exhibits a decline with increasing oxygen saturation. The reason for this is most likely the differences in absorption properties of oxyhemoglobin and reduced hemoglobin.

When an oxygen molecule is attached to a hemoglobin molecule, oxyhemoglobin is formed (HbO_2). A new three-dimensional structure of the hemoglobin molecule consequently generates[15]. Altered molecule structure causes decreased absorption probability for some wavelengths and increased for others. Considering that the wavelength of the emitted light from the LED varies between 775 nm and 825 nm, i.e. not only at the isobestic point, it is not surprising to observe a slight influence of the degree of oxygenation on the recorded forward and side scattering signals.

5.2.4 Osmolarity experiment

The osmolarity is in fact a measure of the osmotic pressure in the blood, caused by the ion concentration inside the cells versus that in the plasma. The primary positive ion in the plasma is Na^+, where it maintains the osmotic pressure[1]. For that reason, the variable parameter in the osmolarity experiments was chosen to be the concentration of NaCl. If water is added to the blood, the water molecules pass through the cell membrane as a consequence of the equalisation of the osmotic pressure. The cellular volume increases and hemolysis eventually occurs when the membrane bursts.

The physiological concentration of Na^+ in the blood is 145 mmol/l[1,24], which corresponds to 9 g/l of NaCl, i.e. 0.9 weight %. In Figure 4.30, both the side and the forward scattering intensities decrease when the NaCl concentration increases. An increase in the ion concentration causes a reduction in the cellular volume. Consequently, it is the scattering properties that are affected by changes in the osmolarity, for instance a decrease in the NaCl concentration increases the cellular volume and accordingly also increases the scattering coefficient μ_s[14]. Due to the high g-factor (g=0.9938)[25], the effective scattering coefficient μ_s' decreases. When studying Figure 4.13 and Figure 4.14, it is seen that an increase in the forward and side scattering signals causes a decrease in μ_s', which is what is shown in Figure 4.31. For dialysis patients, the osmolarity may vary ±5% and in this range, the side scattering intensity varies about ±5% and the forward scattering intensity approximately ±10%. The impact on the recorded signals is greater for NaCl concentrations > 0.9% than for concentrations < 0.9%. This is clearly shown in Figure 4.31, where the ratio S/F is displayed versus the NaCl concentration. If the NaCl concentration decreases by 5%, the ratio decreases by approximately 2%, but if the NaCl concentration increases by the same amount, the ratio increases by almost 7%. Still, the impact of changes in osmolarity is weaker on the ratio compared to on the forward scattering signal.

In Figure 4.32 the interval of the NaCl concentration is expanded to lower values, and the results from the BVS AK 200 measurements are also shown. The values from the BVS AK 200 and from the forward scattering signal of the modified Hemoscan sensor almost coincide. Interesting is also to note that the deviations from the intensities recorded at 0.9% NaCl are more distinct for concentrations less than 0.85%, which is not shown in Figure 4.30. Thus, there appears to be an interval with NaCl concentrations in the range 0.85-0.9%, where the impact on the optical signals is small. Furthermore, it is worth noticing that the impact of the NaCl concentration on the ratio of the side to the forward scattering intensities of the modified sensor is significantly smaller than that on the transmittance of the BVS AK 200.

5.2.5 Flow rate experiments

In Figure 4.34 and Figure 4.35 it is clearly shown that the forward and side scattering signals are affected by the flow rate. The changes in the signals in comparison to that recorded at the flow rate 290 ml/min, varied approximately between -5 and 5%. These signals are also highly influenced by the concentration of total hemoglobin in blood, i.e. the concentration of blood cells. It is noticeable that the flow rate dependence of the recorded signals looks completely different depending on the concentration of blood cells. As can be seen in Figure 4.34 and Figure 4.35, the flow dependence of both the side and forward scattering signals for the lowest concentration of blood cells has a positive slope in contrast to the negative slope found for higher concentrations. However, when forming a ratio (see Figure 4.36) of the side and forward scattering signals for each concentration, no influence of the blood cell concentration on the flow dependence can be observed (Figure 4.37). Interesting is also to note that the flow dependence is considerably reduced when formulating a ratio compared to the side and forward scattering signals. At flow rates up to 290 ml/min, the relative difference is 2-3% and 0.5-1% for flow rates higher than 290 ml/min.

The reasons for the dependence of the flow rate on the recorded signals are probably the changes in the aggregation and alignment of the cells when the flow rate is varied. Since the blood cell is disc shaped, the orientation of the cells in the flowing blood is of high importance. Due to for instance viscosity effects, the alignment and orientation of the cells might vary and this could affect the scattering properties[16,20].

In the comparative study concerning the performance of three sensors, the set-up included a roller pump mounted on the dialysis machine, AK 200. This made it possible to measure at low flow rates (down to 25 ml/min). The side and forward scattering intensities recorded by the modified Hemoscan as well as the transmitted intensity by the BVS AK 200 decreased significantly when reducing the flow rate from 150 to 25 ml/min. This was not observed for the hematocrit values given by the Crit-Line. In Figure 4.38a–c, it can be seen that the slope of the curves is increasing with decreasing hemoglobin concentration. This is confirmed by Table 4.1, listing the slopes of the flow dependence versus the concentration of hemoglobin. However, some data must be neglected here due to difficulties in finding a linear fit to graphs exhibiting large variations. In Figure 4.38a–c it can also be noted that the largest relative change and thus the impact of the flow rate, is obtained for the transmitted intensity of the BVS AK 200. This is even more evident in

Figure 4.39a–c, where the standard deviation of each measurement series is plotted for the three sensors. A large standard deviation indicates a strong influence of the flow rate on the recorded signal. The largest values are obtained for the transmission signal registered by the BVS AK 200, for all hemoglobin concentrations. The standard deviations of the side and forward scattering intensities are both larger than that for the ratio between them. Finally, the standard deviations of the hematocrit values, measured by the Crit-Line, are displayed, revealing small values. However, it is interesting to note that the standard deviation of the S/F-ratio is comparable to that of the Crit-Line hematocrit. This means that forming a ratio of the two signals recorded by the modified Hemoscan, minimises the flow dependence of the signals to such extent that it is comparable to that of a commercially available blood volume sensor.

6. Conclusions

The blood volume sensor (BVS) evaluated in this work is a modification of the Hemoscan BVS, also called the BVS AK 200. The sensor cavity of this original sensor was modified by building in another detector (a photo diode) at right angle to the light source (an LED). In this way, both the light intensity transmitted straight forward and scattering at right angles could be measured. The idea was to investigate these recorded detector signals when several different dialysis-related parameters of the blood were varied. In the evaluation, both a thorough examination of the modified Hemoscan as well as a comparison with other sensors, i.e. the BVS AK 200 and a commercially available BVS (Crit-Line), were performed.

The utilised method is based on optical measurements of changes in the concentration of red blood cells (see section 1.2). When the hematocrit-value of the blood increases, the recorded signal of the original Hemoscan sensor shows an exponential decay, in accordance with the Beer-Lambert law. If the logarithm of the recorded signal is compared with the hematocrit or the hemoglobin concentration, a linear dependence is received. However, if other parameters vary besides the hematocrit-value, such as flow rate, oxygen saturation and osmolarity, the accuracy of this sensor is considerably reduced. Our hope was that these unwanted variations could be excluded by using two detected signals of the modified Hemoscan sensor. A common method when two different signals are available is to form a ratio. In this way, a dimensionless quantity is received and the influence of many parameters can often be reduced.

The sensor cavity and the cuvette used originates from the Hemoscan BVS. Measurement results indicate that the cuvette has a slight conical shape and a various wall thickness when rotating the cuvette. This asymmetrical shape affects the recorded signals of the modified Hemoscan. Thus, concerning the ability to reproduce the received results, it is important that the shaping of the cuvette is improved, especially the angular thickness variation of the wall. The optical properties of the surface of the sensor cavity also affect the recorded signals. When using an absorbing surface, consisting of black paint, the ratio of the side to the forward scattering signals shows a more linear and selective dependence to the hematocrit-value than in the case of a reflecting aluminium surface. However, an absorbing surface also results in a weak forward scattering signal. If the hematocrit is high, there might be a risk of losing the linear response of the photo diode of the forward scattering detector. A suggestion for improvement is to use a more powerful LED or more sensitive photo diodes.

Besides the hemoglobin experiments and the fundamental experiments of the sensor cavity and cuvette, the investigated parameters in this work are hemolysis, oxygen saturation, osmolarity and flow rate. The occurrence of hemolysis is mainly a question of handling the blood with great caution. In our experiments, the oxygen feed was solved by carefully stirring in the blood beaker instead of using the specially designed mini-oxygenator. We also avoided narrow connectors to the PVC tubes and very high flow rates. In this manner, the degree of hemolysis could be minimised. Concerning the degree of oxygen saturation, the impact on the recorded signals is small within reasonable limits. The osmolarity has a higher influence on the detected signals but if

using the ratio S/F, our results indicate that the deviations are small for osmolarity-values corresponding to concentrations of sodium chloride between 0.85 and 0.90 weight %. Beyond these limits, the influence of osmolarity is significant. However, the relative impact on the ratio S/F of the modified Hemoscan is always less than on the transmitted intensity of the BVS AK 200.

The primary advantage by using the ratio S/F is shown in the flow rate experiments. The recorded signals of both the modified Hemoscan sensor and the BVS AK 200 have a complicated dependence to the flow rate but when forming a ratio, this dependence is considerably reduced. Although the flow rate dependence is different when measuring on blood with different hematocrit, the deviations of the ratio S/F are still small. Furthermore, there is a linear dependence between the ratio S/F of the modified Hemoscan and the hematocrit-value monitored by the blood volume sensor, Crit-Line. Even better, the standard deviations of the S/F ratio from the flow rate experiments is comparable the to that of the Crit-Line hematocrit. Thus, our opinion is that the ratio S/F of the modified Hemoscan sensor could be used to build an algorithm monitoring blood volume changes with an accuracy equivalent to that from a commercially available blood volume sensor.

7. Acknowledgements

First of all, we would like to express our gratitude to our supervisor Dr. Annika Enejder. This work would not have been possible without your encouragement and good advice. It has been invaluable having a supervisor who is a true expert in the special field of blood optics, always having answers to our questions and lots of ideas.

We are also very grateful for all the help from the people at the division of Technical Research, Gambro. In the very beginning of our work, we would not have proceeded without the help of Dr. Thomas Hertz and Per-Ola Wictor, concerning the electronics. Special thanks to Roland Persson for designing the logging program (you spared us a lot of suffering!) and to Per Hansson for helping us with the most various things, such as supplying us with the vernier calliper and installing the Hemoscan on the AK 200. At the division of Chemical Research, we would like to thank Lena Järkelid and Evi Martinsson for their help with the plasma separation. We are also grateful to Dr. Jan Sternby, Carina Mathiasson, Ingrid Hjerpe, Yvonne Wismar-Fransson and Dr. Gert-Inge Bertinsson.

Many thanks to Johannes Swartling for designing the Monte Carlo program, and to Dr. Stefan Andersson-Engels for arousing an interest in the field of biomedical optics.

Finally, we would like to thank Prof. Sune Svanberg, whose admirable enthusiasm and pedagogical talent initially led us into the field of applied physics.

8. Reference List

1. "Gambro Basics," Lund, Gambro Lundia AB (1998).

2. R. R. Steuer and J. M. Conis, "The incidence of hypovolemic morbidity in hemodialysis," Dialysis & Transplantation **25,** 272-281 (1996).

3. R. R. Steuer, J. Leypoldt, A. K. Cheung, D. H. Harris, and J. M. Conis, "Hematocrit as an indicator of blood volume and a predictor of intradialytic morbid events," American Society for Artificial Internal Organs **40,** 691-696 (1998).

4. R. R. Steuer, J. K. Leypoldt, A. K. Cheung, H. O. Senekjian, and J. M. Conis, "Reducing symptoms during hemodialysis by continuously monitoring the hematocrit," American Journal of Kidney Diseases **27,** 525-532 (1996).

5. J. P. P. M. de Vries, C. G. Olthof, V. Visser, P. M. Kouw, A. Van es, A. J. M. Donker, and P. M. J. M. de Vries, "Continuous measurements of blood volume during hemodialysis by an optical method," American Society of Artificial Internal Organs Journal **38,** M181-M185 (1992).

6. J. P. P. M. de Vries, A. J. M. Donker, and P. M. J. M. de Vries, "Prevention of hypovolemia-induced hypotension during hemodialysis by means of an optical reflection method," The International Journal of Artificial Organs **17 (4),** 209-214 (1994).

7. J. P. P. M. de Vries, P. M. J. M. de Vries, C. G. Olthof, V. Visser, and P. M. Kouw, "Continuous measurements blood volume using light reflection: Method and validation," Medical & Biological Engineering & Computing **31,** 412-415 (1993).

8. D. Schneditz, H. Pogglitsch, J. Horina, and U. Binswanger, "A blood protein monitor for the continuous measurement of blood volume changes during hemodialysis," Kidney International **38,** 342-346 (1990).

9. B. Tedner and L. E. Lins, "Fluid volume changes during hemodialysis monitored with the impedance technique," Artificial Organs **9,** 416-420 (1985).

10. C. Johner, P. W. Chamney, D. Chneditz, and M. Ramer, "Evaluation of an ultrasonic blood volume monitor," **13,** 2098-2103 (1998).

11. P. O. Wictor and B. Petterson, "An in vitro method for continuous measurements of blood volume changes during haemodialysis," Lund, Lund Institute of Technology (1994).

12. W. Nienstedt, O. Hänninen, A. Arstila, and S.-E. Björkqvist, "Människans fysiologi och anatomi," Uppsala, Almqvist & Wiksell (1994).

13. C. K. Mathews and K. E. van Holde, "Biochemistry," Redwood city, California, The Benjamin/Cummings Publishing Company, Inc. (1990).

14. P. D. Wimberley, N. Fogh-Andersen, O. Siggaard-Andersen, F. C. Lundsgaard, and W. G. Zijlstra, "Effect of pH on the absorption spectrum of human oxyhemoglobin: A potential source of error in measuring the oxygen saturation of hemoglobin," Clinical Chemistry **34,** 750-754 (1988).

15. A. M. K. Enejder, "Light scattering and absorption in tissue - models and measurements," Lund, Lund Institute of Technology, Department of Physics (1997).

16. L.-G. Lindberg and P. Å. Öberg, "Optical properties of blood in motion," Optical engineering **32,** 253-257 (1993).

17. A. J. Welch and J. C. van Gemert, "Optical-thermal response of laser-irradiated tissue," New York, Plenum Press (1995).

18. H. C. van de Hulst, "Light scattering by small particles," New York, Dover Publications, Inc. (1981).

19. E. Hecht, "Optics," Addison-Wesley publishing company, Inc. (1987).

20. P. Alsholm, "Light scattering by individual and groups of spheroidal particles," Lund, Lund institute of technology, Department of Physics (1996).

21. F. Paolini, E. Mancini, A. Bosetto, and A. Santoro, "Hemoscan: a dialysis machine-integrated blood volume monitor," Artificial Organs **18,** 487-494 (1995).

22. T. Murata, "Effects of sedimentation of small red blood cell aggregates on blood flow in narrow horizontal tubes," Biorheology **33,** 267-283 (1996).

23. M. R. Mueller, H. Schima, H. Engelhardt, A. Salat, D. B. Olsen, U. Losert, and E. Wolner, "In vitro hematological testing of rotary blood pumps: remarks on standardization and data interpretation," Artificial Organs **17,** 103-110 (1993).

24. C. Ekelius and J. Svensson, "An optical transmission method for continuous measurement of blood volume changes during haemodialysis," Lund, Lund Institute of Technology, Department of Physics (1994).

25. A. Roggan, M. Friebel, K. Dörschel, A. Hahn, and G. Müller, "Optical properties of circulating human blood," in *Laser-tissue interaction and tissue optics*, G. P. Delacretaz, G. Godlewski, R. Pini, R. W. Steiner, and L. O. Svaasand, eds., Proc. Soc. Photo-Opt. Instr. Eng. **3195**-09 (SPIE Bellingham, 1998)

9. Appendix

Modifications of the electronics:

1. Pin 4 at contact P4 (Hospal) was connected to pin 4 at contact P1 (Hospal). (CHSDARK connected to ground.)

2. Changes to synchronise the protective system with the control system:

a) Pin 10 at U11 (Hospal CS) was connected to pin 9 at U3 (Hospal PS). (The synchronisation of the new photo diode.)
b) Pin 8 at U11 (Hospal CS) was connected to pin 8 at U3 (Hospal PS). (The synchronisation of the new photo diode.)
c) Pin 8 and 10 at U4 (Hospal PS) was connected. (No need for the clock of the protective system anymore.)
d) Pin 7 at U5 (Hospal PS) was connected to R48 (Hospal CS), the reference signal.

3. A potentiometer was added on the ADC-card with the following connections:

a) The pin in the middle of the potentiometer (ADC-card) was connected to pin 3 at IC7 (ADC-card).
b) The pin on the potentiometer intended for 0 V was connected to Z5VR (ADC-card)
c) The pin on the potentiometer intended for 5 V was connected to pin 4 at IC3 (ADC-card).
d) Pin 2 at contact P3 (ADC-card) was connected to pin 7 at U2 (Hospal).

The following contacts were used to connect the Hospal card with the master card:

- P1 at the Hospal card was connected to P3 at the master card.
- P2 at the Hospal card was connected to P5 at the master card.
- P3 at the Hospal card was connected to P2 at the master card.